Wind Park and Wind Turbine Models in EMTP®

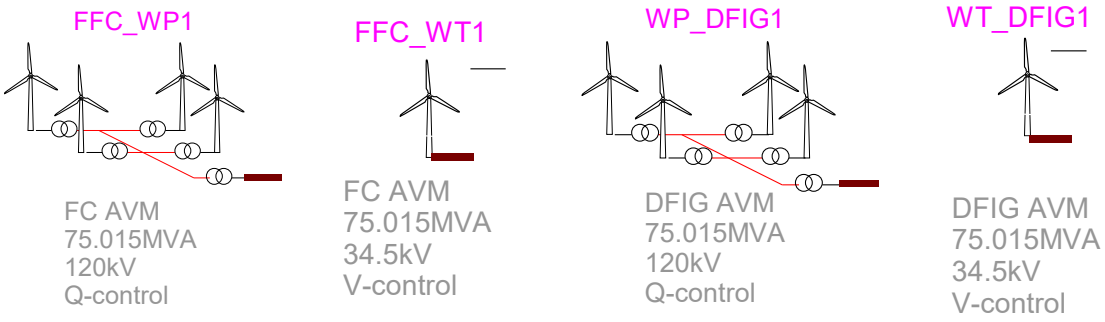

2021-06-10 11:56:00 AM

Prepared by:
Ulas Karaagac, Hossein Ashourian, Anton Stepanov, Henry Gras, Jean Mahseredjian

TABLE OF CONTENTS

Table of Figures

Objective

This document presents generic EMT-type models for full size converter (FSC) and Doubly-fed induction generator (DFIG) based wind parks (WPs) that can be used for stability analysis and interconnection studies. These models are developed in EMTP Version 3.4 and above.

1 INTRODUCTION

The large scale wind parks (WPs) employ variable speed wind turbines (WTs) in order to increase energy capture, reduce drive train stresses and comply with grid code requirements. Doubly-fed induction generator (DFIG) and full size converter (FSC) WTs fall into this category.

Interconnecting a large-scale WP into the bulk power system has become a more important issue due to its significant impact on power system transient behavior. Failure to perform proper interconnection studies could lead to not only non-optimal designs and operations of WPs, but also severe power system operation and even stability problems. Manufacturer-specific models of WPs are typically favored for the interconnection studies due to their accuracy. However, these WP models have been typically delivered as black box models and their usage is limited to the terms of nondisclosure agreements. Utilities and project developers require accurate generic WP models to perform the preliminary grid integration studies before the actual design of the WP is decided. Accurate generic WP models will also enable the researchers to identify the potential WP grid integration issues and propose necessary countermeasures.

This document presents EMT-type models for FSC and DFIG based WPs that can be used for stability analysis and interconnection studies. In the aggregated WP model, the collector grid and the WTs are represented with their aggregated models. However, the model includes the wind park controller to preserve the overall control structure in the WP. The WT and the WP control systems include the necessary nonlinearities, transient and protection functions to simulate the accurate transient behavior of the WP to the external power system disturbances.

The first part of this document briefly presents the FSC and DFIG based WPs. The developed EMTP models are presented in the second part. The last part presents the illustrative simulation examples.

2 WIND PARKS WITH VARIABLE SPEED WIND TURBINES

A simplified single line diagram of a typical wind park is shown in Figure 1. In wind parks, WTs are connected through a step-up transformer (WT transformer) to the medium voltage (MV) collector bus by means of subterranean cables. The collector bus voltage is stepped up to the high voltage (HV) level by means of wind park transformer. Depending on the selection of the function, either the reactive power or voltage or power factor at the point of interconnection (POI in Figure 1) is controlled by a central wind park controller (WPC) located at wind park substation. The wind park transformer usually contains an on load tap changer (OLTC) to maintain nominal voltage at MV collector bus.

The available reactive power at the point of interconnection (POI) is usually much less than the specified WT capacity due to the reactive power losses at the WT transformers, the medium voltage (MV) collector grid and the wind park transformer. Therefore, reactive power compensation may be required to fulfill the grid code requirements regarding power factor control [1].

The EMT model presented in this document does not include the wind park transformer OLTC and any reactive power compensation device (such as Static VAR Compensator).

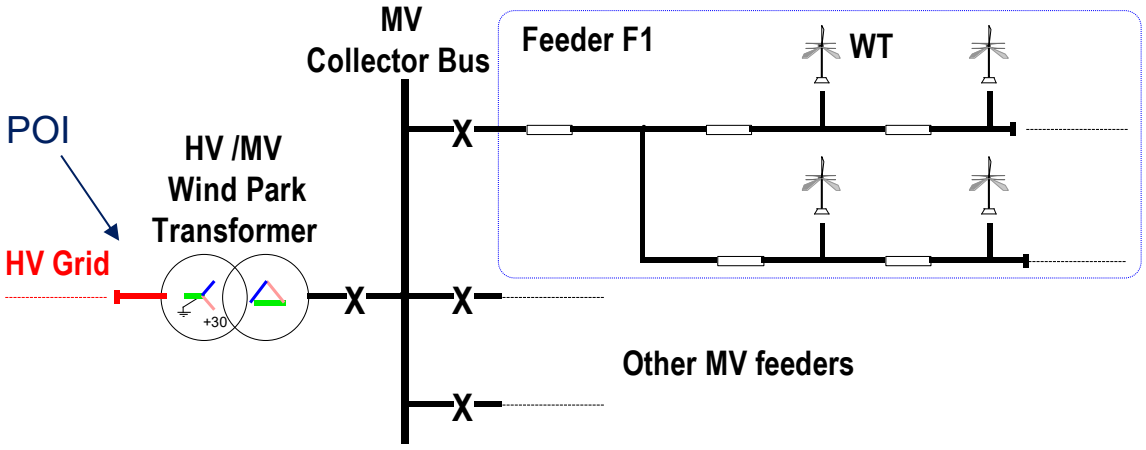

Figure 1 Simplified single-line diagram of a typical wind park

2.1 Variable Speed Wind Turbines

As the size of the WTs increase, the WT technology has switched from fixed speed to variable speed. The drivers behind these developments are mainly increasing the energy capture, reducing the drive train stresses and ability to comply with the grid code requirements. Most common configurations are FSC and DFIG WTs [2].

2.1.1 Wind Turbine Aerodynamics

The wind turbine extracts kinetic energy from the swept area of the blades. The mechanical power extracted from the wind is given by [2]:

$$P_t = \frac{1}{2}\rho A\upsilon^3 C_p(\lambda,\beta) \qquad (1)$$

where ρ is the air density (approximately 1.225 kg/m^3), A is the swept area of the rotor (m^2), υ is upwind free wind speed (m/s) and C_p is the power coefficient.

C_p is a characteristic of the WT and is usually provided as a set of curves (C_p curves) relating C_p to tip-speed-ratio λ with the blade pitch angle β as a parameter, as shown in Figure 2 [3]. The tip-speed-ratio is defined as

$$\lambda = (\omega_t R)/\upsilon \tag{2}$$

where ω_t is the WT rotational speed (rad/s) and R is the blade radius (m).

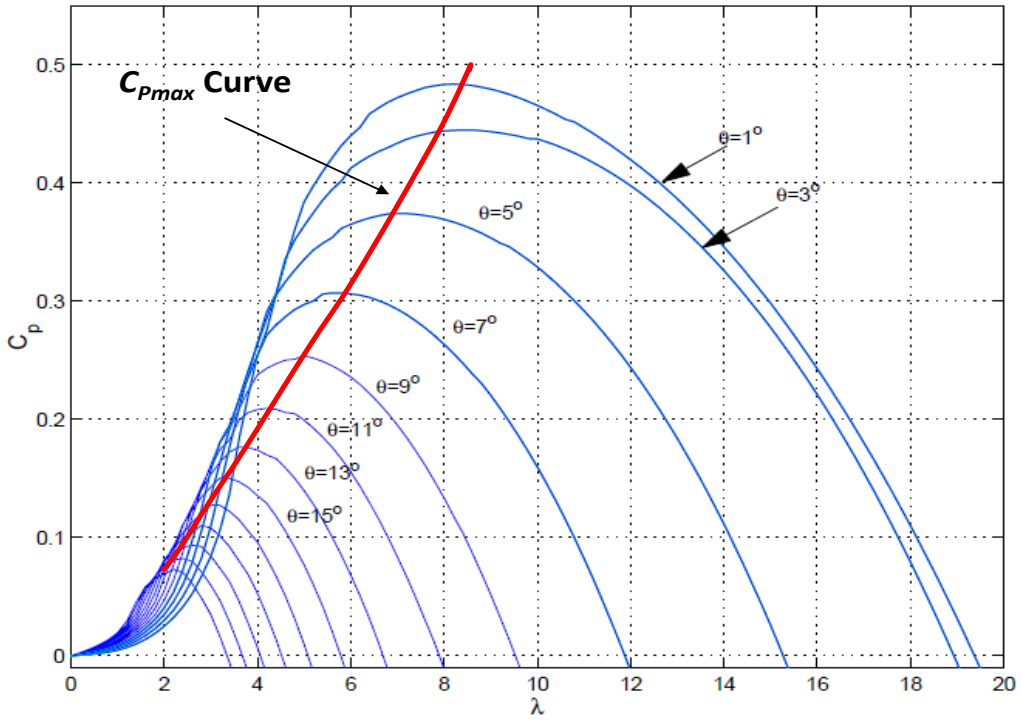

Figure 2 Wind power C_p curves

At a specific wind speed and pitch angle, there is a unique WT rotational speed that achieves the maximum power coefficient C_{p-max}, hence the maximum mechanical power as shown in Figure 2.

The mathematical model of the WT aerodynamics is shown in Figure 3. In this modeling approach, the C_p curves of the WT are fitted with high order polynomials on λ and β, as follows

$$C_p(\lambda,\beta) = \sum_{i=1}^{n}\sum_{j=1}^{n}\alpha_{ij}\lambda^i\beta^j \tag{3}$$

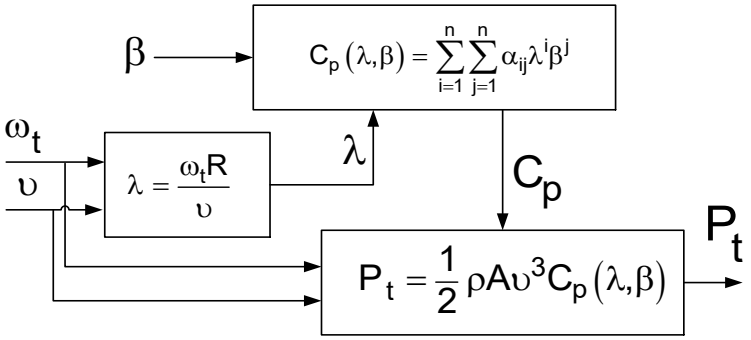

Figure 3 Wind turbine model for aerodynamics

2.1.2 Mechanical System

The mechanical system is constituted by the blades linked to the hub, coupled to the slow shaft, which is linked to the gearbox which multiplies the rotational speed of the fast shaft connected to the generator. Although the mechanical representation of the entire WT is complex, representing the fundamental resonance frequency of the drive train using its two mass model is sufficient as the other resonance frequencies are much higher and their magnitudes are lower [4]. By referring all magnitudes in the fast shaft (generator side), the state space equations of the two mass system can be written as

$$\dot{\bar{\omega}}_t = (1/J_t)\left(\bar{T}_t - D_{tg}\left(\bar{\omega}_t - \omega_g\right) - D_t\ \bar{\omega}_t - K_{tg}\left(\bar{\theta}_t - \theta_g\right)\right) \quad (4)$$

$$\dot{\bar{\theta}}_t = \bar{\omega}_t \quad (5)$$

$$\dot{\omega}_g = (1/J_g)\left(K_{tg}\left(\bar{\theta}_t - \theta_g\right) - D_{tg}\left(\omega_g - \bar{\omega}_t\right) - D_g\ \omega_g - T_g\right) \quad (6)$$

$$\dot{\theta}_g = \omega_g \quad (7)$$

where $\bar{\omega}_t$, $\bar{\theta}_t$, $\bar{T}_t$ are the rotor speed (rad/s), angular position of the rotor (rad) and the aerodynamic torque (Nm) of the WT referred to the fast shaft, respectively. ω_g, θ_g, T_g are the speed, angular position and electromagnetic torque of the generator, respectively. J_t and D_t are the moment of inertia (kgm^2) and absolute speed self-damping coefficient (Nms/rad) of the WT referred to the fast shaft, respectively. J_g and D_g are the moment of inertia and absolute speed self-damping coefficient of the generator, respectively. K_{tg} and D_{tg} are the equivalent spring constant (Nm/rad) and mutual damping coefficient (Nms/rad), between the WT and the generator, respectively.

2.1.3 Control of Variable Speed Wind Turbines

The control of variable speed WT calculates the generator power output and the pitch angle in order to achieve extracting the maximum energy from the wind and keeping the WT in safe operating mode. The WT remains shut down when the wind speed is too low for energy production (i.e. below cut-in speed υ_{cut-in}). When the wind speed is above υ_{cut-in} and below rated speed υ_{rated}, the pitch angle is kept at zero ($\beta = 0^0$) and the power reference of the WT generator is produced by the MPPT (maximum power point tracking) function to achieve optimal operation. The conventional method is calculating the power reference using a cubic function of the turbine angular speed.

$$P_{ref} = K_{opt}\ \omega_t^3 \quad (8)$$

where

$$K_{opt} = (1/2)C_{p-max}\ \rho\ A\left(R\ /\lambda_{opt}\right)^3 \quad (9)$$

When the wind speed is above υ_{rated}, the pitch angle is increased by the pitch controller (see Figure 4) in order to limit the mechanical power extracted from the wind and reduce the mechanical loads on the drive train. The pitch controller should ensure zero pitch angle ($\beta = 0^0$) for the wind speeds below υ_{rated} [5]. When the wind speed is above cut-off speed $\upsilon_{cut-off}$, the WT is shut down.

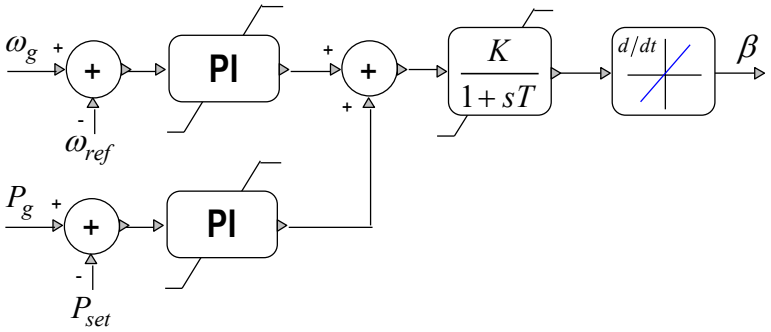

Figure 4 Schematic diagram of pitch control

2.2 Reactive Power Control in Wind Parks with Variable Speed Wind Turbines

The active power at the point of interconnection (POI in Figure 1) depends on the wind conditions at each WT inside the WP and determined by MPPT function (see (8)) when the wind speed is between υ_{cut-in} and υ_{rated}. However, according to customary grid code requirements, the WP should have a central wind park controller (WPC) to control the reactive power at POI.

The WP reactive power control is based on the secondary voltage control concept [6]. At primary level, the WT controller (WTC) monitors and controls its own positive sequence terminal voltage (V_{wt}^{+}) with a proportional voltage regulator. At secondary level, the WPC monitors the reactive power at POI (Q_{POI}) and control it by modifying the WTC reference voltage values (V') via a proportional-integral (PI) reactive power regulator as shown in Figure 5. In Figure 5 and hereafter, all variables are in pu (unless otherwise stated) and the apostrophe sign is used to indicate the reference values coming from the controllers.

Although not shown in Figure 5, the WPC may also contain voltage control (V-control) and power factor control (PF-control) functions. When the WPC is working under V-control function, the reactive power reference in Figure 5 (Q'_{POI}) is calculated by an outer proportional voltage control, i.e.

$$Q_{POI} = K_{Vpoi}\left(V'_{POI} - V^{+}_{POI}\right) \qquad (10)$$

where V^{+}_{POI} is the positive sequence voltage at POI and K_{Vpoi} is the WPC voltage regulator gain.

When WPC is working under PF-control function, Q'_{POI} is calculated using the active power at POI (P_{POI}) and the desired power factor at POI (pf_{POI}).

When a severe voltage sag occurs at POI (due to a fault), the PI regulator output ($\Delta U'$) is kept constant by blocking the input ($Q'_{POI} - Q_{POI}$) to avoid overvoltage following the fault removal.

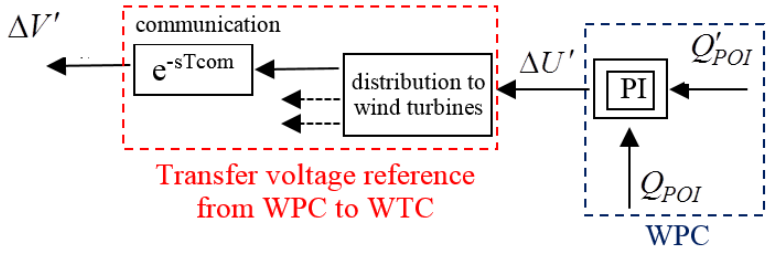

Figure 5 Reactive power control at POI (Q-control function)

2.3 Full Size Converter (FSC) Wind Turbines

FSC WT may or may not have a gearbox and a wide range of electrical generators such as asynchronous, conventional synchronous and permanent magnet can be employed. As all the WT power is transferred through an ac-dc-ac converter system, the specific characteristics and dynamics of the electrical generator are effectively isolated from the grid [7].

The considered topology in this paper is shown in Figure 6. It uses a permanent magnet synchronous generator (PMSG) and the ac-dc-ac converter system consists of two voltage source converters (VSCs): machine side converter (MSC) and grid side converter (GSC). The dc resistive chopper is used for the dc bus overvoltage protection. Although not shown in Figure 6, a line inductor (choke filter) and an ac harmonic filter are used at the GSC to improve the power quality.

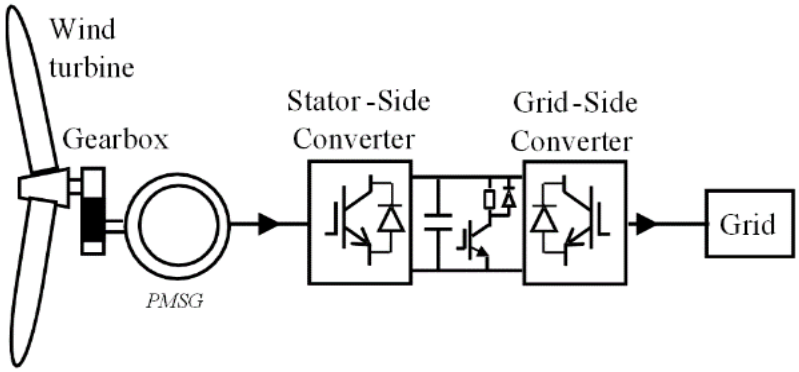

Figure 6 FSC wind turbine configuration

The simplified diagram of FSC WT control and protection system is shown in Figure 7. The sampled signals are converted to per unit and filtered at “Measurements & Filters” block. The input measuring filters are low-pass (LP) type. “Compute Variables” block computes the variables used by the FSC WT control and protection system. “Pitch Control” block (see Figure 4) limits the mechanical power extracted from the wind by increasing the pitch angle when the wind speed is above its rated. “Protection System” block contains cut-in and cut-off speed relays, low voltage and overvoltage relays, MSC and GSC overcurrent protections and dc resistive chopper control.

The control of the FSC WT is achieved by controlling the MSC and GSC utilizing vector control techniques. Vector control allows decoupled control of real and reactive powers. The currents are projected on a rotating reference frame based on either ac flux or voltage. Those projections are referred to d- and q- components of their respective currents. In flux-based rotating frame, the q-component corresponds to real power and the d-component to reactive power. In voltage-based rotating frame (90^0 ahead of flux-based frame), the d and q components represent the opposite.

The control scheme is illustrated in Figure 8. In this figure, i_{qm} and i_{dm} are the q- and d-axis currents of the MSC, i_{qg} and i_{dg} are the q- and d-axis currents of the GSC, V_{dc} is the dc bus voltage, T is the electromagnetic torque of the PMSM, and V_{wt}^{+} is the positive sequence voltage at FSC transformer MV terminal.

In the control scheme presented in Figure 8, the MSC operates in the stator flux reference (SFR) frame and the GSC operates in the stator voltage reference (SVR) frame. i_{qm} is used to control T, i_{dg} is used to maintain V_{dc} and i_{qg} is used to control V_{wt}^{+}.

Both MSC and GSC are controlled by a two-level controller. The slow outer control calculates the reference dq-frame currents (i'_{dm}, i'_{qm}, i'_{dg} and i'_{qg}) and the fast inner control allows controlling the converter ac voltage reference that will be used to generate the modulated switching pattern.

The reference for PMSM electromagnetic torque is given by MPPT control ($T' = K_{opt}\ \omega_t^2$) and the reference for the positive sequence voltage at FSC transformer MV terminal (V') is calculated by the WPC (see Figure 5).

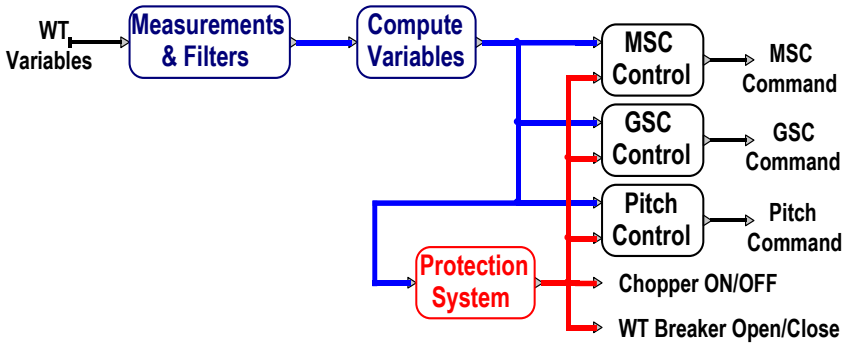

Figure 7 Simplified diagram of FSC WT control and protection system

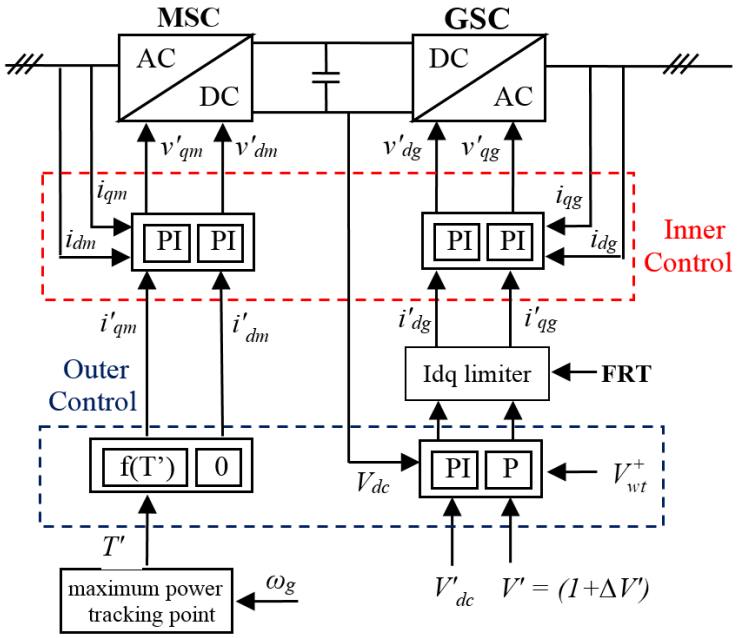

Figure 8 Schematic diagram of FSC WT control

2.4 Doubly-Fed Induction Generator (DFIG) Wind Turbines

In WTs with DFIG, the stator of the induction generator (IG) is directly connected to the grid and the wound rotor is connected to the grid through an ac-dc-ac converter system as shown in Figure 9. The ac-dc-ac converter system consists of two voltage source converters (VSCs): rotor side converter (RSC) and grid side converter (GSC). A line inductor and shunt harmonic ac filters are used at the GSC to improve power quality (not shown in Figure 9). A crowbar is used to protect the RSC against overcurrent and the dc capacitor against overvoltage. During crowbar ignition, the RSC is blocked and the IG consumes reactive power. To avoid the crowbar ignition during faults, the dc resistive chopper is widely used to limit the dc voltage. DFIG WT also includes the protection functions presented in Section 2.3.

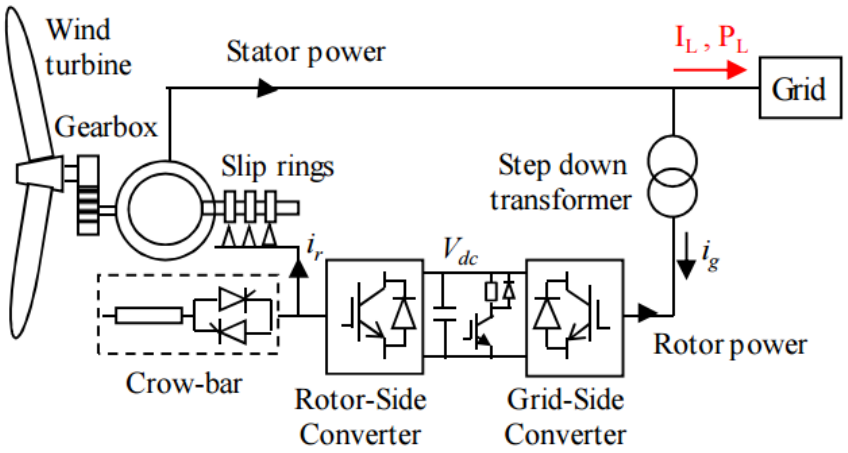

Figure 9 DFIG wind turbine configuration

The overall control and protection scheme in DFIG WT is similar to the one in FSC WT shown in Figure 7. The sampled signals are converted to per unit and filtered at the “Measurements & Filters” block. The input measuring filters are low-pass (LP) type. The “Compute Variables” block computes the variables used by the DFIG WT control and protection system. The “Pitch Control” block (see Figure 4) limits the mechanical power extracted from the wind by increasing the pitch angle when the wind speed is above its rated. However, the “Protection System” block contains crowbar protection in addition to the cut-in and cut-off speed relays, low voltage and overvoltage relays, RSC and GSC overcurrent protections and dc resistive chopper control. It should be noted that, the crowbar protection is not expected to operate unless the dc resistive chopper protection is deactivated.

The DFIG converter control scheme is illustrated in Figure 10. In this figure, i_{qr} and i_{dr} are the q- and d-axis currents of the RSC, i_{qg} and i_{dg} are the q- and d-axis currents of the GSC, V_{dc} is the dc bus voltage, P is the active power output of the DFIG, and V_{wt}^{+} is the positive sequence voltage at DFIG transformer MV terminal. The RSC operates in SFR frame and the GSC operates in SVR frame. i_{qr} and i_{dr} are used to control P and V_{wt}^{+}, respectively. On the other hand, i_{dg} is used to maintain the dc bus voltage (V_{dc}) and i_{qg} is used to support the grid with reactive power during faults.

Both RSC and GSC are controlled by a two-level controller. The slow outer control calculates the reference dq-frame currents (i'_{dr}, i'_{qr}, i'_{dg} and i'_{qg}) and the fast inner control allows controlling the converter ac voltage reference.

The reference for DFIG active power output (P') is given by MPPT control (see (8)). The reference for DFIG positive sequence voltage (V') is calculated by the WPC (see Figure 5).

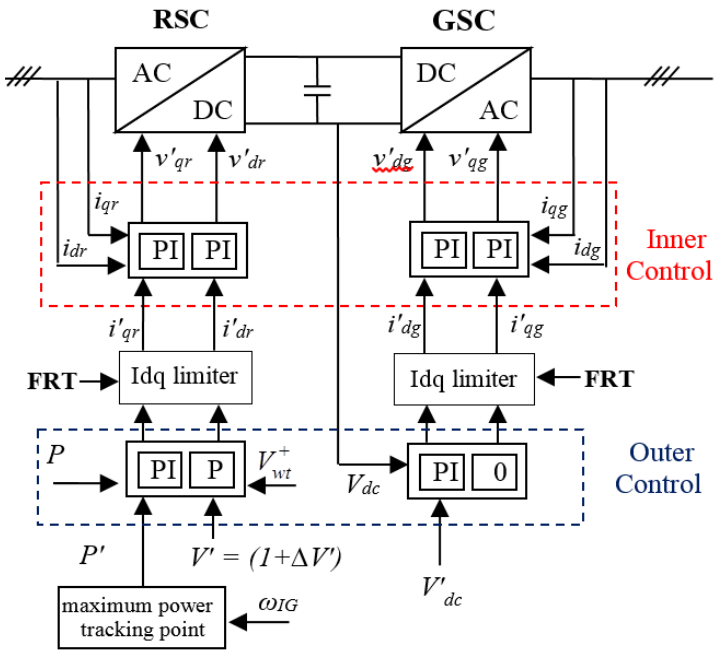

Figure 10 Schematic diagram of DFIG WT control

3 EMTP IMPLEMENTATION

The developed wind park model setup in EMTP is encapsulated using a subcircuit with a programmed mask as illustrated in Figure 11 and Figure 12. The model consists of a wind turbine, a LV/MV wind turbine transformer, equivalent PI circuit of the collector grid and a MV/HV wind park transformer.

The first tab of the wind park mask enables the user to modify the general wind park parameters (number of WTs in the WP, POI and collector grid voltage levels, collector grid equivalent and zig-zag transformer parameters (if it exists)), the general wind turbine parameters (WT rated power, voltage and frequency), and wind park operating conditions (number of WTs in service, wind speed WPC operating mode and reactive power (or power factor) at POI).

The second and the third tab is used for MV/HV WP transformer and LV/MV WT transformer parameters, respectively.

The forth tab is used to modify the parameters of converter control system given below:

- Sampling rate and PWM frequency at WT converters
- WT input measuring filter parameters,
- MSC (or RSC) control parameters,
- GSC control parameters,
- Coupled / Decoupled sequence control option for GSC

The fifth tab is used to modify the parameters of voltage sag, chopper, crowbar (for DFIG only) and overcurrent protections. The sixth tab is used to modify the WPC parameters.

The associated JavaScript file (DFIG_WP_Parameters.dwj and FC_WP_Parameters.dwj, for DFIG and FSC based WP, respectively) computes the internal model parameters. It also contains the data that is not accessible from the mask, such as the data for WT aerodynamics, mechanical system and pitch control.

The wind farm transformer connection is wye-grounded on the HV side and Delta on the MV side. The WT transformer connection is wye-grounded on the LV side and Delta on the MV side. In both transformers the magnetizing branch is located at the Delta connection side.

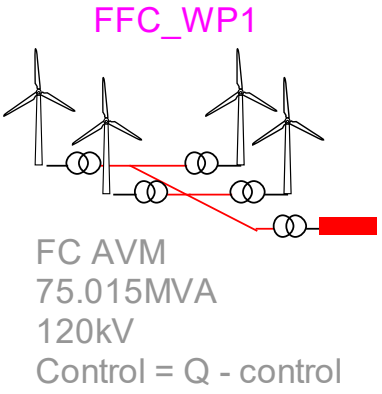

Figure 11 FSC based wind park device, mask parameters shown in Figure 12

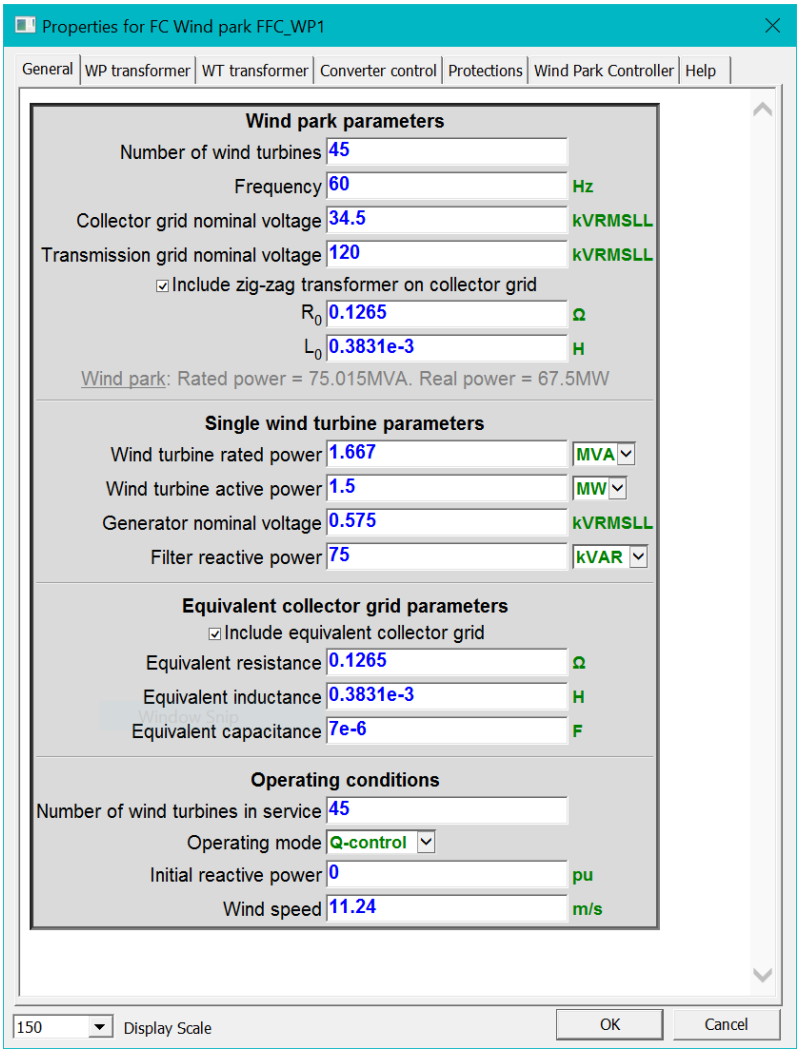

Figure 12 FSC based wind park device mask

3.1 Detailed and Average Value Models

The EMTP diagram of the wind turbine ac-dc-ac converter system detailed model (DM) is shown in Figure 13. A detailed two-level topology (Figure 14.a) is used for the VSCs in which the valve is composed by one IGBT switch, two non-ideal (series and anti-parallel) diodes and a snubber circuit as shown in Figure 14.b. The non-ideal diodes are modeled as non-linear resistances. The DC resistive chopper limits the DC bus voltage and is controlled by the protection system block.

The PWM block in the ac-dc-ac converter system EMTP diagram receives the three-phase reference voltages from converter control and generates the pulse pattern for the six IGBT switches by comparing the voltage reference with a triangular carrier wave. In a two-level converter, if the reference voltage is higher than the carrier wave then the phase terminal is connected to the positive DC terminal, and if it is lower, the phase terminal is connected to the negative DC terminal. The EMTP diagram of the PWM block is presented in Figure 15.

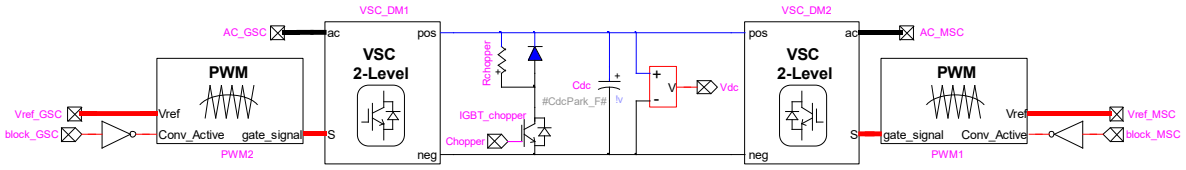

Figure 13 EMTP® diagram of ac-dc-ac converter system block in WT models (detailed model version)

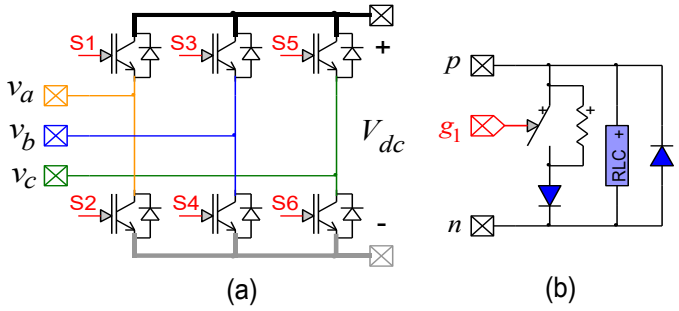

Figure 14 (a) Two-level Converter, (b) IGBT valve

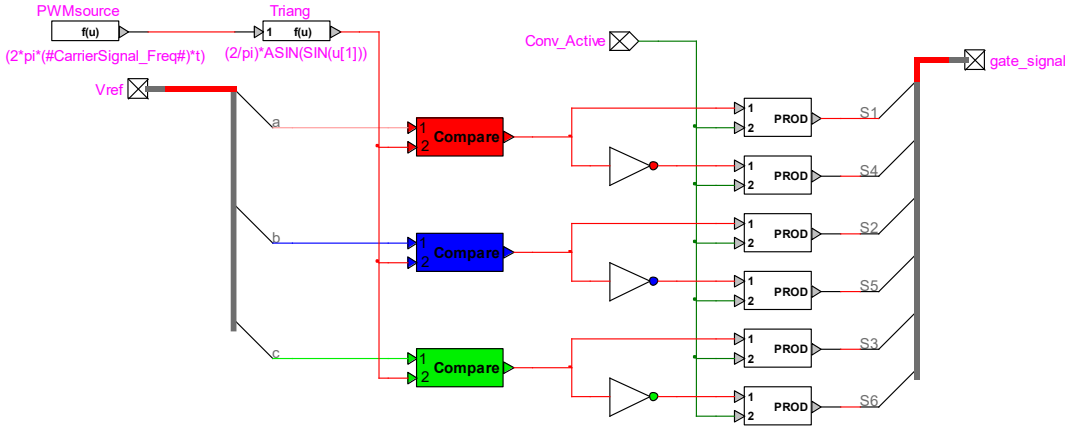

Figure 15 PWM control block

The DM mimics the converter behavior accurately. However, the simulation of such switching circuits with variable topology requires many time consuming mathematical operations and the high frequency PWM signals force small simulation time step usage. These computational inefficiencies can be eliminated by using the average value model (AVM) which replicates the average response of switching devices, converters and controls through simplified functions and controlled sources [8]. AVMs have been successfully developed for wind generation technologies [9], [10]. The AVM obtained by replacing the DM of converters with voltage-controlled sources on the ac side and current-controlled sources on the dc side, as shown in Figure 16 and Figure 17.

The forth (converter control) tab of the wind park device mask (see Figure 12) enables used AVM-DM selection.

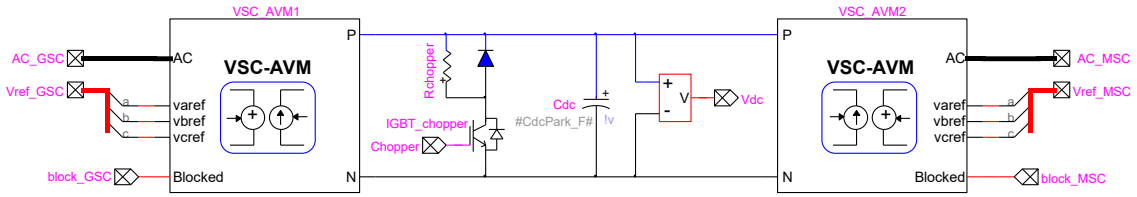

Figure 16 EMTP® diagram of ac-dc-ac converter system block in WT models (average value model version)

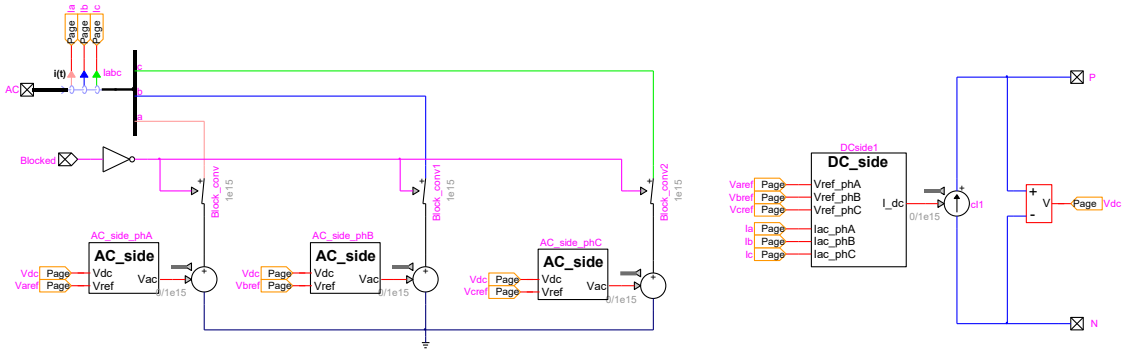

Figure 17 AVM Representation of the VSC

3.2 FSC based Wind Park Model in EMTP®

The EMTP® diagram of the FSC based Wind Park is shown in Figure 18. It is composed of

- "Wind Turbine" block,
- "WT Electrical System" block,
- "WT Control System" block,
- "WP Control System" block,
- PI circuit that represents equivalent collector grid,
- Wind park transformer,
- Initialization Source with load flow (LF) constraint.

The "Wind Turbine" block contains wind turbine aerodynamics given in Figure 3 and the mechanical system model given by (4) - (7).

The initialization source contains the load flow constraint. It also prevents large transients at external network during initialization of WT electrical and control systems.

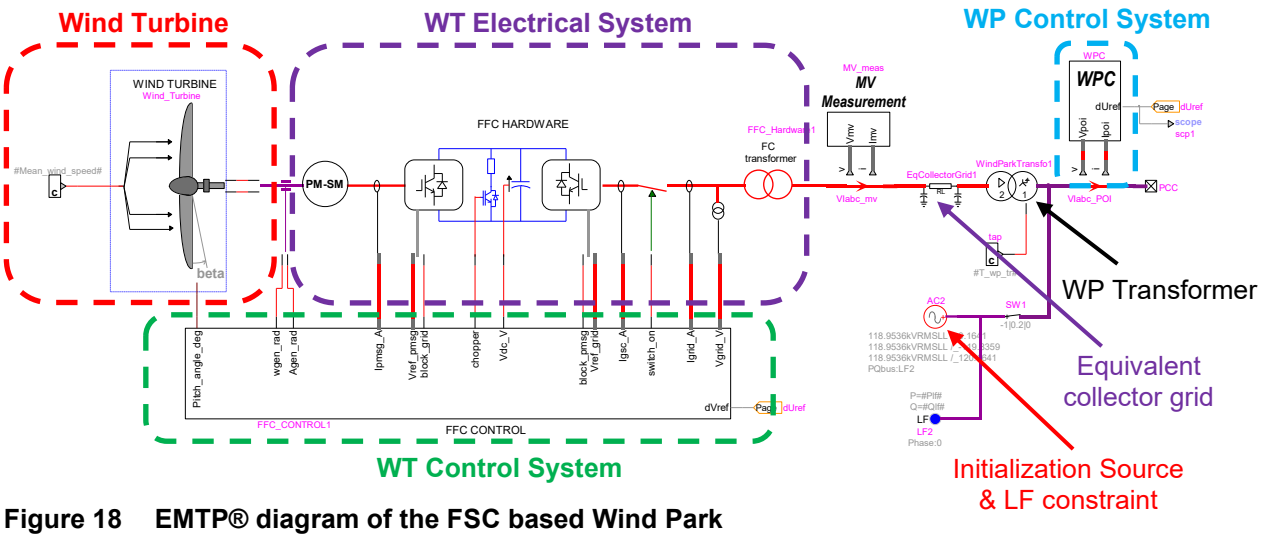

Figure 18 EMTP® diagram of the FSC based Wind Park

3.2.1 Wind Park Control System Block

The function of WPC is to adjust the WT controller voltage reference in order to achieve desired reactive power at POI (see Figure 5). The “WP Control System” block consists a measuring block, an outer voltage (or power factor) control and a slow inner proportional-integral reactive power control as shown in Figure 19. The measuring block receives the voltages and the currents at POI (i.e. HV terminal of wind farm transformer) and calculates the voltage magnitude, active power and reactive power. The reactive power reference for the inner proportional-integral reactive power control is produced either by the outer proportional voltage control (V-control) or by the outer power factor control (pf-control) unless Q-control is selected.

Similar to the “Wind Turbine” block, the “WP Control System” block is identical in both FSC and DFIG based WPs.

3.2.2 FSC Wind Turbine Electrical System Block

The EMTP diagram of the “WT Electrical System” block is composed of PMSM, ac-dc-ac converter system, choke filter, shunt ac harmonic filters and WT transformer, as shown in Figure 20.

The measurement blocks are used for monitoring and control purposes. The monitored variables are MSC, GSC and total FC currents, and FC terminal voltages. The dc voltage is also monitored (in ac-dc-ac converter system block) as well as the PMSM electromagnetic torque. All variables are monitored as instantaneous values and meter locations and directions are shown in Figure 20.

The ac-dc-ac converter system block details have been presented in Section 3.1.

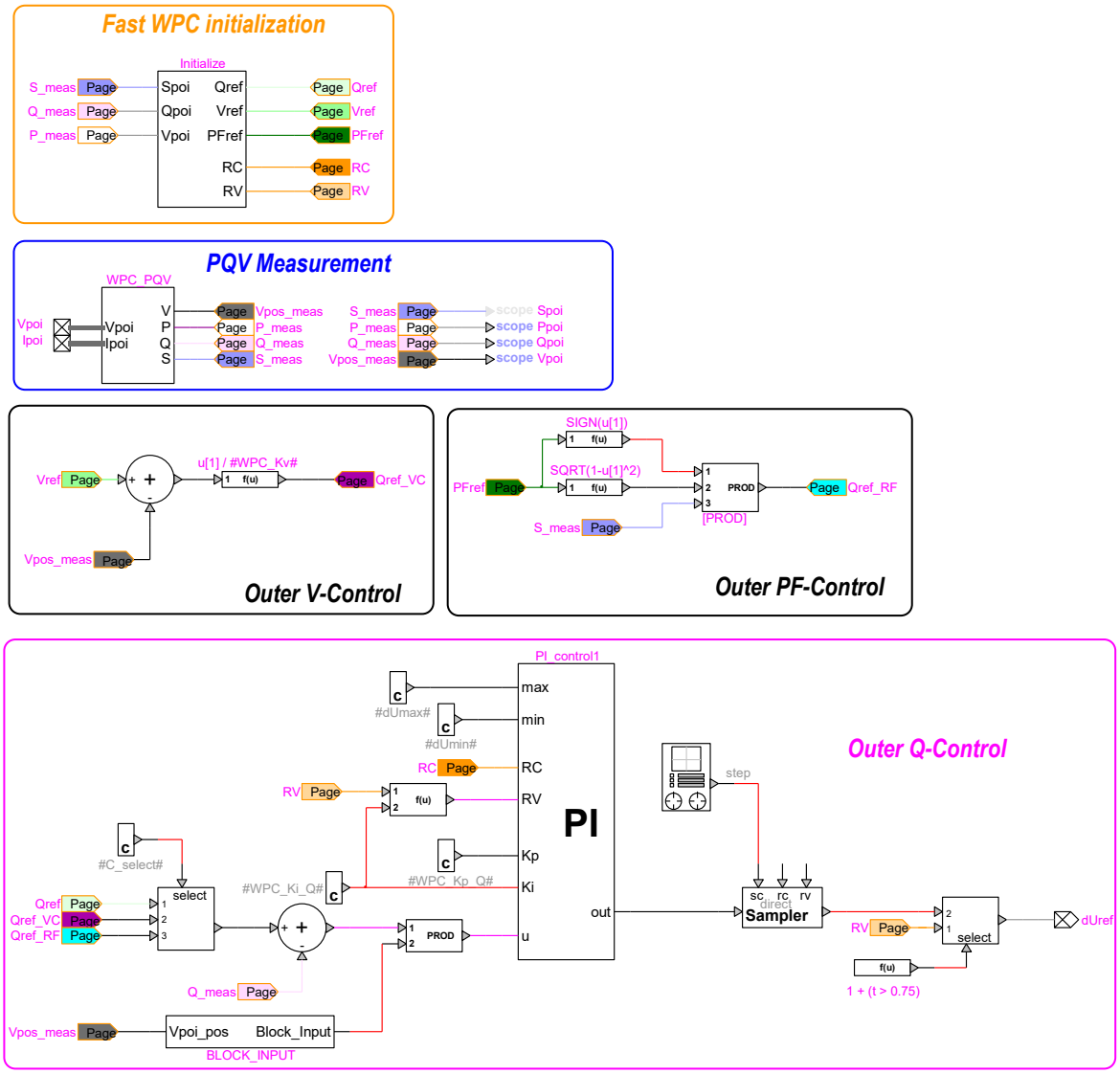

Figure 19 EMTP® diagram of "WP Control System" block

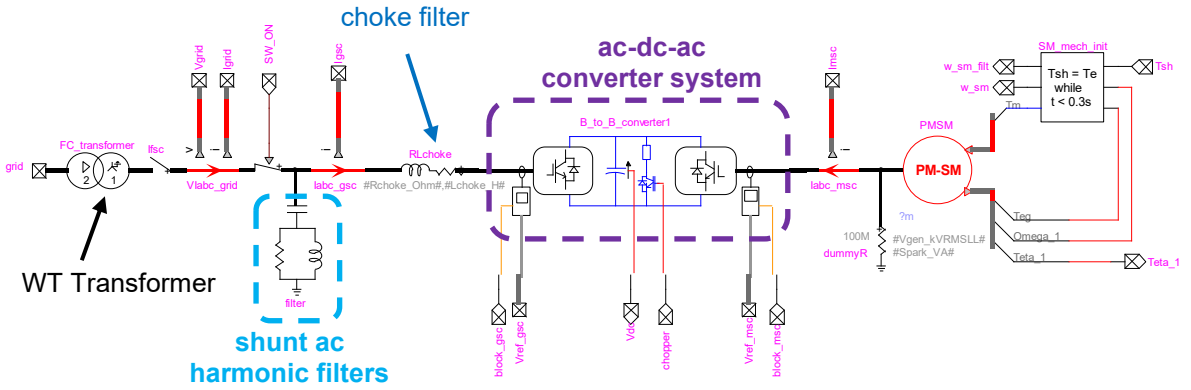

Figure 20 EMTP® diagram of FSC "WT Electrical System" block

The “shunt ac harmonic filters” block includes two band-pass filters as shown in Figure 21. These filters are tuned at switching frequencies harmonics n_1 and n_2. The filter parameters are computed as

$$C_{f1} = \frac{Q_{filter}\ N_{wt}}{U^2(2\pi f)} \tag{11}$$

$$L_{f1} = \frac{N_{wt}}{C_{f1}(2\pi f\ n_1)^2} \tag{12}$$

$$R_{f1} = \frac{(2\pi f)n_1\ L_{f1}\ Q}{N_{wt}} \tag{13}$$

$$C_{f2} = C_{f1} \tag{14}$$

$$L_{f2} = \frac{N_{wt}}{C_{f2}(2\pi f\ n_2)^2} \tag{15}$$

$$R_{f2} = \frac{(2\pi f)n_2\ L_{f2}\ Q}{N_{wt}} \tag{16}$$

where U is the rated LV grid voltage, Q_{filter} is the reactive power of the filter and Q is the quality factor with a value of 1000.

The switching frequencies harmonics n_1 and n_2 are as follows

$$n_1 = f_{PWM-gsc}/f_s \tag{17}$$

$$n_2 = 2n_1 \tag{18}$$

where $f_{PWM-gsc}$ is the PWM frequency at GSC and f_s is the nominal frequency.

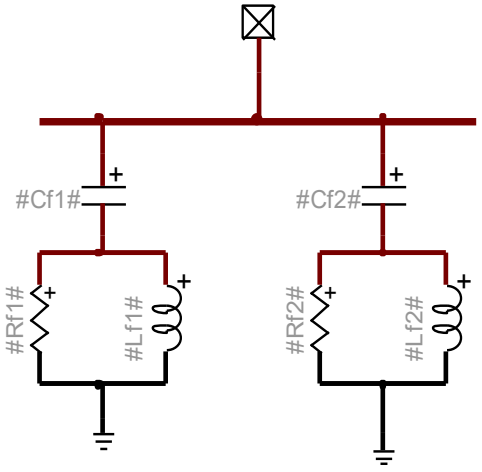

Figure 21 “shunt ac harmonic filter” block

3.2.3 FSC Wind Turbine Control System Block

The EMTP diagram of the FSC WT control system block is shown in Figure 22. The sampled signals are converted to pu and filtered. The sampling frequencies are set to 12.5 kHz for both MSC and GSC from device mask as shown in Figure 12. The “sampling” blocks are deactivated in AVM due to large simulation time step usage. In the generic model, 2nd order Bessel type low pass filters are used. The cut-off frequencies of the filters are set to 2.5 kHz for both MSC and GSC. However, the order (up to 8th order), the type (Bessel and Butterworth) and the cut-off frequencies of the low pass filters can be modified from the device mask as shown in Figure 12. The “MSC Compute Variables” and

"GSC Compute Variables" blocks do the dq transformation required for the vector control. The MSC control ("PMSG Control" block) operates in the stator flux reference frame and the GSC ("Grid Control" block) operates in the stator voltage reference frame. The pitch control is activated when the wind speed increases above the rated value and given in Figure 4. The protection block includes the over/under voltage relay, the deep voltage sag detector, the dc chopper control and overcurrent detector.

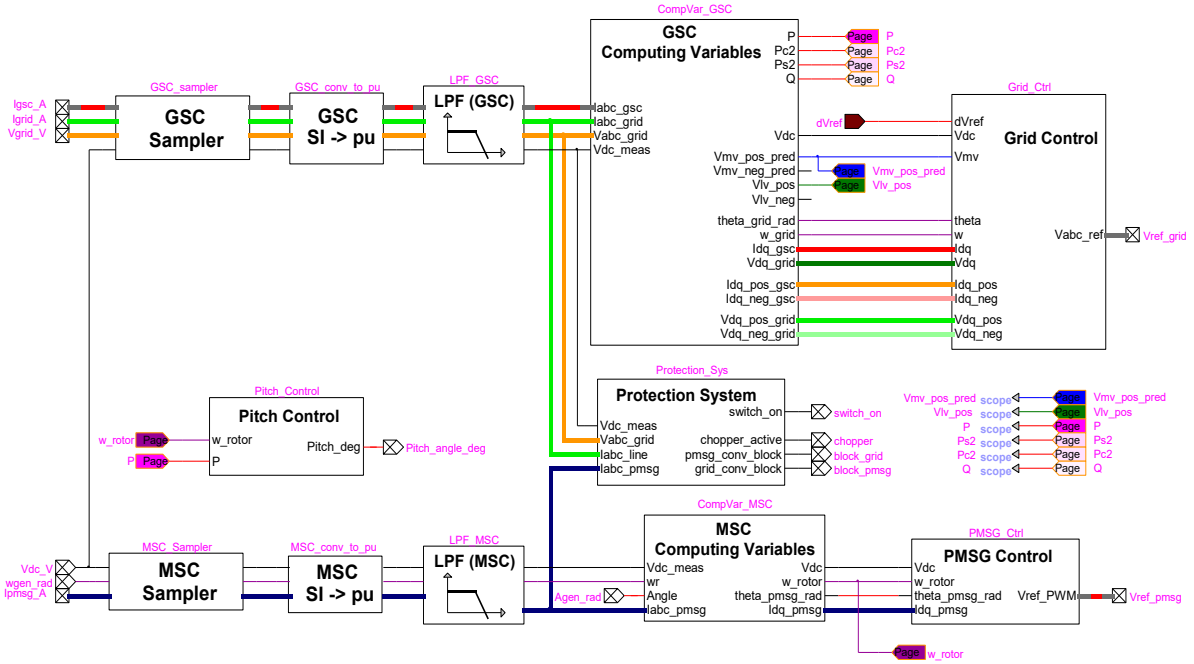

Figure 22 EMTP® diagram of FSC "WT Control System" block

The transformation matrix T in (19) transforms the phase variables into two quadrature axis (d and q reference frame) components rotating at synchronous speed $\omega = d\theta / dt$. The phase angle θ of the rotating reference frame is derived by the double synchronous reference frame (DSRF) PLL [11] (see Figure 23) from the FSC WT terminal voltages allowing the synchronization of the control parameters with the system voltage. In matrix the following T, the direct axis d is aligned with the stator voltage.

$$T = \frac{2}{3}\begin{bmatrix} \cos(\omega t) & \cos(\omega t - 2\pi/3) & \cos(\omega t + 2\pi/3t) \\ -\sin(\omega t) & -\sin(\omega t - 2\pi/3) & -\sin(\omega t + 2\pi/3) \\ 1/2 & 1/2 & 1/2 \end{bmatrix} \qquad (19)$$

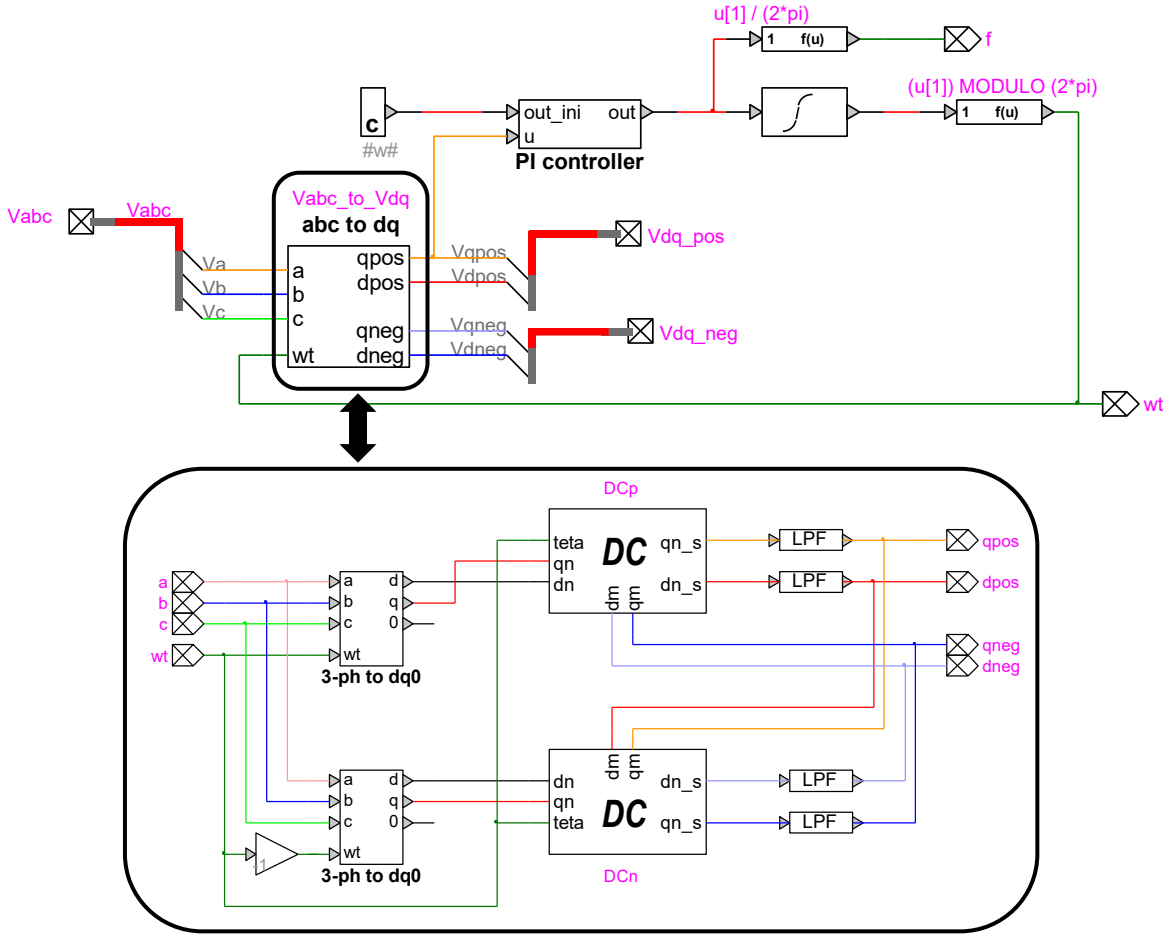

Figure 23 EMTP® diagram of DSRF PLL

3.2.3.1 FSC Machine Side Converter Control

The EMTP diagram of the “PMSG Control” block is shown in Figure 24. The function of the MSC is to control the electromagnetic torque of the PMSM.

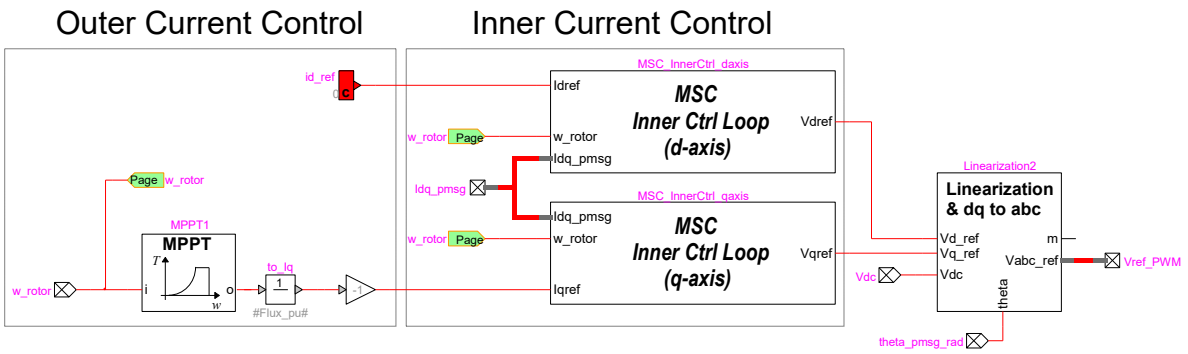

Figure 24 EMTP® diagram of FSC “PMSG Control” block

The d-axis current reference is set to zero ($i'_{dm} = 0$) to achieve unity power factor. The q-axis current reference is given by

$$i'_{qm} = T'/\lambda_m \qquad (20)$$

where λ_m is the constant flux generated by the permanent magnet and $T'(=K_{opt}\,\omega_t^2)$ is the reference for PMSM electromagnetic torque given by the MPPT control.

The MSC inner control loop is designed based on internal model control (IMC) method. This method results dq-frame proportional integral (PI) or PI-type controllers, the parameters (gain and integration time) of which are expressed directly in certain machine parameters and the desired closed-loop bandwidth. This simplifies the controller design procedure, eliminating or reducing the need for trial-and-error [12].

The PMSG stator voltages are found from

$$v_{dm} = -R_s i_{dm} - L_d\left(d\,i_{dm}/dt\right) + \omega_g L_q i_{qm} \tag{21}$$

$$v_{qm} = -R_s i_{qm} - L_q\left(d\,i_{qm}/dt\right) + \omega_g\left(L_d i_{dm} + \lambda_m\right) \tag{22}$$

where R_s is the armature resistance, L_d and L_q are the d- and q-axis inductances of PMSG.

The i_{dm} and i_{qm} errors are processed by the PI controller to give v_{dm} and v_{qm}, respectively. To ensure good tracking, feed-forward compensating terms $\omega_g L_q i_{qm}$ in (21) and $\omega_g\left(L_d i_{dm} + \lambda_m\right)$ in (22) are added. The converter reference voltages become

$$v'_{dm} = -\left(k_p^d + k_i^d/s\right)\left(i'_{dm} - i_{dm}\right) + \omega_g L_q i_{qm} \tag{23}$$

$$v'_{qm} = -\left(k_p^q + k_i^q/s\right)\left(i'_{qm} - i_{qm}\right) + \omega_g\left(L_d i_{dm} + \lambda_m\right) \tag{24}$$

Using IMC [12],

$$F_{msc}(s) = \frac{\alpha_c}{s} G_{msc}{}^{-1}(s) = \begin{bmatrix} k_p^d + k_i^d/s & 0 \\ 0 & k_p^q + k_i^q/s \end{bmatrix} \tag{25}$$

where $G_{msc}(s)$ is the transfer function that describes the link between MSC output current and voltage, and α_c is the bandwidth. $G_{msc}(s)$ is given by

$$G_{msc}(s) = \begin{bmatrix} R_s + sL_d & 0 \\ 0 & R_s + sL_q \end{bmatrix}^{-1} \tag{26}$$

The relationship between the bandwidth and the rise time (10%–90%) is $\alpha_c = \ln(9)/t_{rise}$.

The PI controller parameters are found as

$$k_p^d = \alpha_c L_d \tag{27}$$

$$k_p^q = \alpha_c L_q \tag{28}$$

$$k_i^d = k_i^q = \alpha_c R_s \tag{29}$$

The PI controller parameters are calculated for the MSC rise time given in the device mask.

3.2.3.2 FSC Grid Side Converter Control

The function of GSC is maintaining the dc bus voltage V_{dc} at its nominal value and controlling the positive sequence voltage at MV side of FSC WT transformer (V_{wt}^+).The EMTP diagram of the “Grid Control” block is shown in Figure 25. The GSC control offers both coupled and decoupled sequence

control options. The user can select the GSC control option from the device mask as shown in Figure 12.

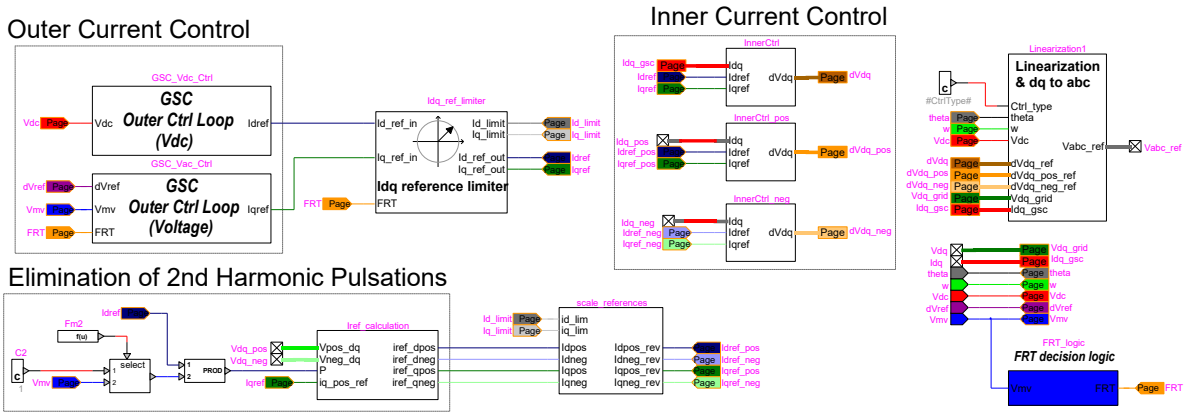

Figure 25 EMTP® diagram of FSC "Grid Control" block

3.2.3.2.1 FSC GSC Coupled Control

The q-axis reference current is calculated by the proportional outer voltage control, as follows

$$i'_{qg} = K_V \left(V' - V^+_{wt} \right) \tag{30}$$

where K_V is the voltage regulator gain. The reference for MV side of FSC WT transformer positive sequence voltage (V') is calculated by the WPC (see Figure 5).

The positive sequence voltage at MV side of FSC WT transformer is not directly measured by the WT controller and it is approximated by

$$V^+_{wt} = \left(V^+_{dwt} \right)^2 + \left(V^+_{qwt} \right)^2 \tag{31}$$

where

$$V^+_{dwt} = \tilde{V}^+_{dwt} + R_{tr} \tilde{I}^+_{dwt} - X_{tr} \tilde{I}^+_{qwt} \tag{32}$$

$$V^+_{qwt} = \tilde{V}^+_{qwt} + R_{tr} \tilde{I}^+_{qwt} + X_{tr} \tilde{I}^+_{dwt} \tag{33}$$

In (31) - (33), V^+_{dwt} and V^+_{qwt} are the d-axis and q-axis positive sequence voltage at MV side of FSC WT transformer, $\tilde{V}^+_{dwt}$ and $\tilde{V}^+_{qwt}$ are the d-axis and q-axis positive sequence voltage at FSC WT terminals (i.e. the d-axis and q-axis positive sequence voltage at LV side of FSC WT transformer), $\tilde{I}^+_{dwt}$ and I^+_{qwt} are the d-axis and q-axis positive sequence currents of FSC WT (i.e. the d-axis and q-axis positive sequence currents at LV side of FSC WT transformer), R_{tr} and X_{tr} are the resistance and reactance values FSC WT transformer.

The d-axis reference current is calculated by the proportional outer dc voltage control. It is a PI controller tuned based on inertia emulation.

$$k_p = \omega_0^2 \left(2H_{Cdc} \right) \tag{34}$$

$$k_i = 2\xi\omega_0 \left(2H_{Cdc} \right) \tag{35}$$

where ω_0 is the natural frequency of the closed loop system and ξ is the damping factor. $H_{Cdc} = (E_{Cdc}/S_{wt})$ is the static moment of inertia, E_{Cdc} is the stored energy in dc bus capacitor (in Joules) and S_{wt} is the wind park rated power (in VA).

The schematic of the GSC connected to the power system is shown in Figure 26. $Z = R + j\omega L$ represents the grid impedance including the transformers as well as the choke filter of the GSC. The voltage equation is given by

$$\mathbf{v_{abc}} = \mathbf{R}\,\mathbf{i_{gabc}} - \mathbf{L}\left(d\,\mathbf{i_{gabc}}/dt\right) + \mathbf{v_{gabc}} \tag{36}$$

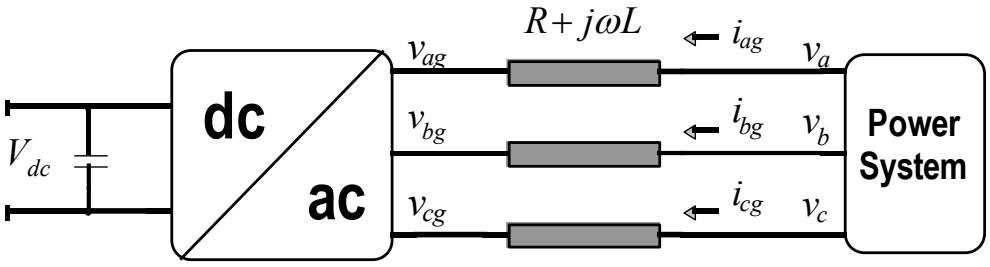

Figure 26 GSC arrangement

The link between GSC output current and voltage can be described by the transfer function

$$G_{gsc}(s) = 1/(R + sL) \tag{37}$$

Using (25), the PI controller parameters of the inner current control loop are found as

$$k_p = \alpha_c L \tag{38}$$

$$k_i = \alpha_c R \tag{39}$$

The PI controller parameters are calculated for the GSC rise time given in the device mask.

Similar to the MSC, the feed-forward compensating terms $\omega L_{choke} i_{qg} + v_{d-choke}$ and $\left(-\omega L_{choke} i_{dg} + v_{q-choke}\right)$ are added to the d- and q-axis voltages calculated by the PI regulators, respectively. The converter reference voltages are as follows

$$v'_{dg} = -\left(k_p + k_i/s\right)\left(i'_{dg} - i_{dg}\right) + \omega L_{choke} i_{qg} + v_{d-choke} \tag{40}$$

$$v'_{qg} = -\left(k_p + k_i/s\right)\left(i'_{qg} - i_{qg}\right) - \omega L_{choke} i_{dg} + v_{q-choke} \tag{41}$$

During normal operation, the controller gives the priority to the active currents, i.e.

$$\begin{aligned} i'_{dg} &< I_{dg}^{lim} \\ i'_{qg} &< I_{qg}^{lim} = \sqrt{\left(I_g^{lim}\right)^2 - \left(i'_{dg}\right)^2} \end{aligned} \tag{42}$$

where I_{dg}^{lim}, I_{qg}^{lim} and I_g^{lim} are the limits for d-axis, q-axis and total GSC currents, respectively.

The WTs are equipped with an FRT function to fulfill the grid code requirement regarding voltage support shown in Figure 27. The FRT function is activated when

$$\left|1 - V_{wt}^{+}\right| > V_{FRT-ON} \tag{43}$$

and deactivated when

$$\left|1-V_{wt}^{+}\right| < V_{FRT-OFF} \tag{44}$$

after a pre-specified release time t_{FRT}.

When the FRT function is active, the GSC controller gives the priority to the reactive current by reversing the d- and q-axis current limits given in (42), i.e.

$$\begin{aligned} i'_{qg} &< I_{qg}^{lim} \\ i'_{dg} &< I_{dg}^{lim} = \sqrt{\left(I_{g}^{lim}\right)^2 - \left(i'_{qg}\right)^2} \end{aligned} \tag{45}$$

The EMTP diagram of “Idq reference limiter” and “FRT decision logic” blocks are given in Figure 28 and Figure 29, respectively. The limits for d-axis, q-axis and total GSC currents and FRT function thresholds can be modified from the device mask.

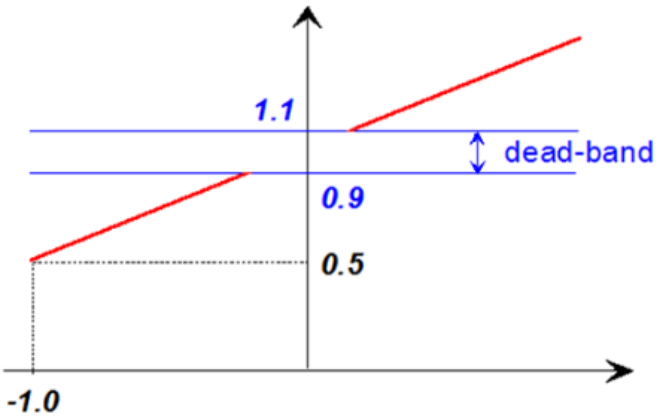

Figure 27 Wind turbine reactive output current during voltage disturbances [13].

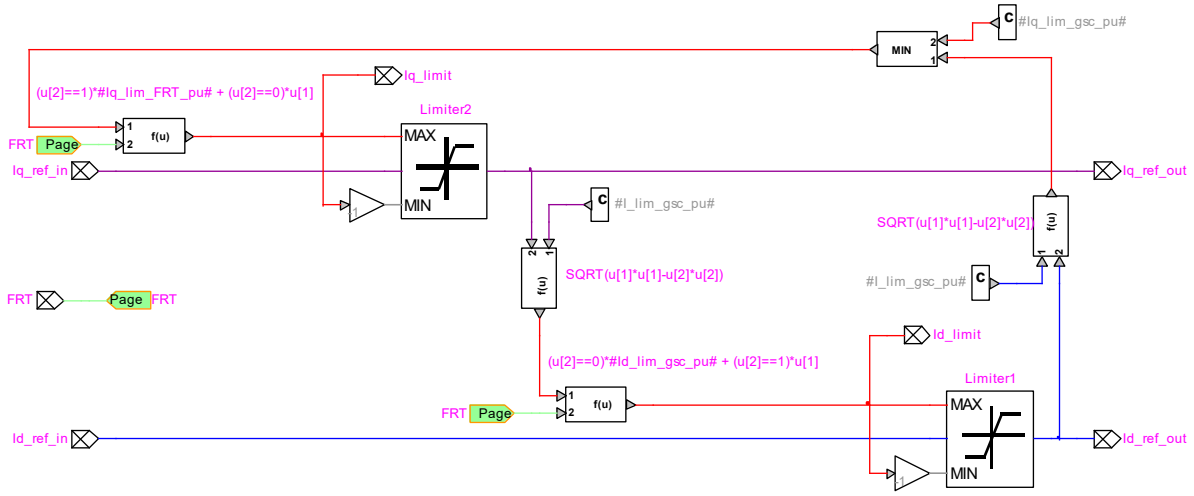

Figure 28 EMTP® diagram of “Idq reference limiter” block

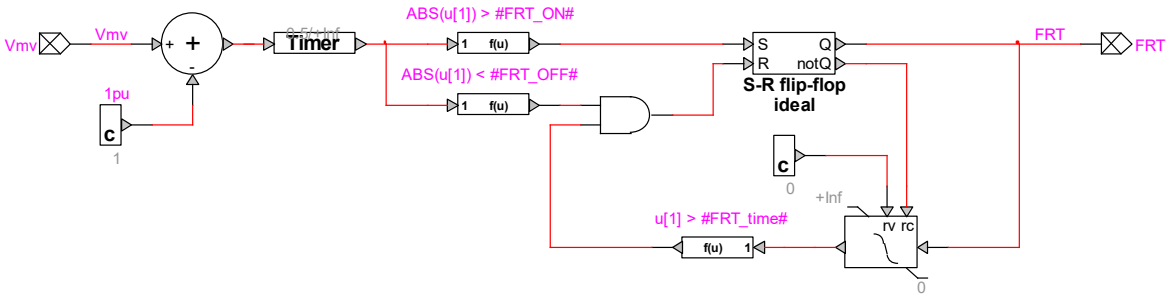

Figure 29 EMTP® diagram of "FRT decision logic" block

3.2.3.2.2 FSC Grid Side Converter Decoupled Sequence Control

Ideally, the GSC control presented in the previous section is not expected to inject any negative sequence currents to the grid during unbalanced loading conditions or faults. However, the terminal voltage of FSC WT contains negative sequence components during unbalanced loading conditions or faults. This causes second harmonic power oscillations in GSC power output. The instantaneous active and reactive powers such unbalanced grid conditions can be also written as [14]

$$\begin{aligned} p &= P_0 + P_{C2}\cos(2\omega t) + P_{S2}\cos(2\omega t) \\ q &= Q_0 + Q_{C2}\cos(2\omega t) + Q_{S2}\cos(2\omega t) \end{aligned} \tag{46}$$

where P_0 and Q_0 are the average values of the instantaneous active and reactive powers respectively, whereas P_{C2}, P_{S2}, Q_{C2} and Q_{S2} represent the magnitude of the second harmonic oscillating terms in these instantaneous powers.

With decoupled sequence control usage, four of the six power magnitudes in (46) can be controlled for a given grid voltage conditions. As the oscillating terms in active power P_{C2}, P_{S2} cause oscillations in dc bus voltage V_{dc}, the GSC current references ($i_{dg}^{+\prime}$, $i_{qg}^{+\prime}$, $i_{dg}^{-\prime}$, $i_{qg}^{-\prime}$) are calculated to cancel out these terms (i.e. $P_{C2} = P_{S2} = 0$).

The outer control and Idq limiter shown in Figure 8 calculates i'_{dg}, i'_{qg}, I_{dg}^{lim} and I_{qg}^{lim}. These values are used to calculate the GSC current references $i_{dg}^{+\prime}$, $i_{qg}^{+\prime}$, $i_{dg}^{-\prime}$ and $i_{qg}^{-\prime}$ for the decoupled sequence current controller. As the positive sequence reactive current injection during faults is defined by the grid code (see Figure 27), the GSC current reference calculation in [14] is modified as below:

$$\begin{bmatrix} i_{qg}^{+\prime} \\ i_{dg}^{+\prime} \\ i_{qg}^{-\prime} \\ i_{dg}^{-\prime} \end{bmatrix} = \begin{bmatrix} 1 & 0 & 0 & 0 \\ v_{qg}^{+} & v_{dg}^{+} & v_{qg}^{-} & v_{dg}^{-} \\ v_{qg}^{-} & v_{dg}^{-} & v_{qg}^{+} & v_{dg}^{+} \\ -v_{dg}^{-} & v_{qg}^{-} & v_{dg}^{+} & -v_{qg}^{+} \end{bmatrix}^{-1} \begin{bmatrix} i'_{qg} \\ P_0 \\ P_{C2} \\ P_{S2} \end{bmatrix} \tag{47}$$

where P_0 is approximated by

$$P_0 = V_{wt}^{+}\, i'_{dg} \tag{48}$$

The calculated reference values in (47) is revised considering the converter limits I_{dg}^{lim} and I_{qg}^{lim}. For example when $\left(i_{qg}^{+\prime} + i_{qg}^{-\prime}\right) > I_{qg}^{lim}$, the q-axis reference current references are revised as below

$$i_{qg}^{+}{}'' = i_{qg}^{+}{}' \left[I_{qg}^{lim} \Big/ \left(i_{qg}^{+}{}' + i_{qg}^{-}{}' \right) \right]$$
$$i_{qg}^{-}{}'' = i_{qg}^{-}{}' \left[I_{qg}^{lim} \Big/ \left(i_{qg}^{+}{}' + i_{qg}^{-}{}' \right) \right] \quad (49)$$

where I_{qg}^{+}" and I_{qg}^{-}" are the revised reference values for q-axis positive and negative currents, respectively.

The revised d-axis positive and negative current references I_{dg}^{+}" and I_{dg}^{-}" can be obtained with the same approach using I_{dg}^{lim}. It should be emphasized here that, during faults the priority is providing I_{dg}^{+} specified by the grid code. The remaining reserve in GSC is used for eliminating P_{C2} and P_{S2}. Hence, its performance reduces with the decrease in electrical distance between the WP and the unbalanced fault location.

As i_{dg}^{+}, i_{qg}^{+}, i_{dg}^{-} and i_{qg}^{-} are controlled, the decoupled sequence control contains four PI regulator and requires sequence extraction for GSC currents and voltages. The sequence decoupling method [15] shown in Figure 30 is used in EMTP implementation. In this method, a combination of a low-pass filter (LPF) and double line frequency Park transform (P^{-2} and P^{+2}) is used to produce the oscillating signal, which is then subtracted. The blocks C and P represent the Clarke and Park transformation matrices, and the superscripts ±1 and ±2 correspond to direct and inverse transformation at line frequency and double line frequency, respectively.

In EMTP implementation, the feed-forward compensating terms $\left(\omega L_{choke} i_{qg} + v_{d-choke}\right)$ and $\left(-\omega L_{choke} i_{dg} + v_{q-choke}\right)$ are kept in coupled form and added to the PI regulator outputs in stationary αβ-frame.

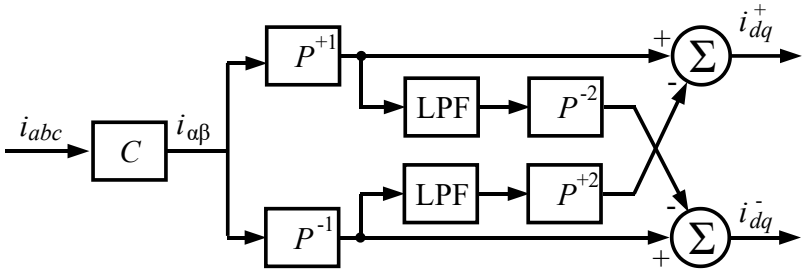

Figure 30 Sequence extraction using decoupling method.

3.2.4 FSC Protection System Block

Figure 31 shows the “protection system” block. It includes overvoltage and undervoltage protection relays, a dc overvoltage protection (chopper protection) and an overcurrent detector for each converter to protect IGBT devices when the system is subjected to overcurrent. For initialization, all protection systems, except for DC chopper protection, are activated after 100ms of simulation (i.e. init_Prot_delay = 0.1s). The protection system parameters can be modified from the device mask as shown in Figure 32.

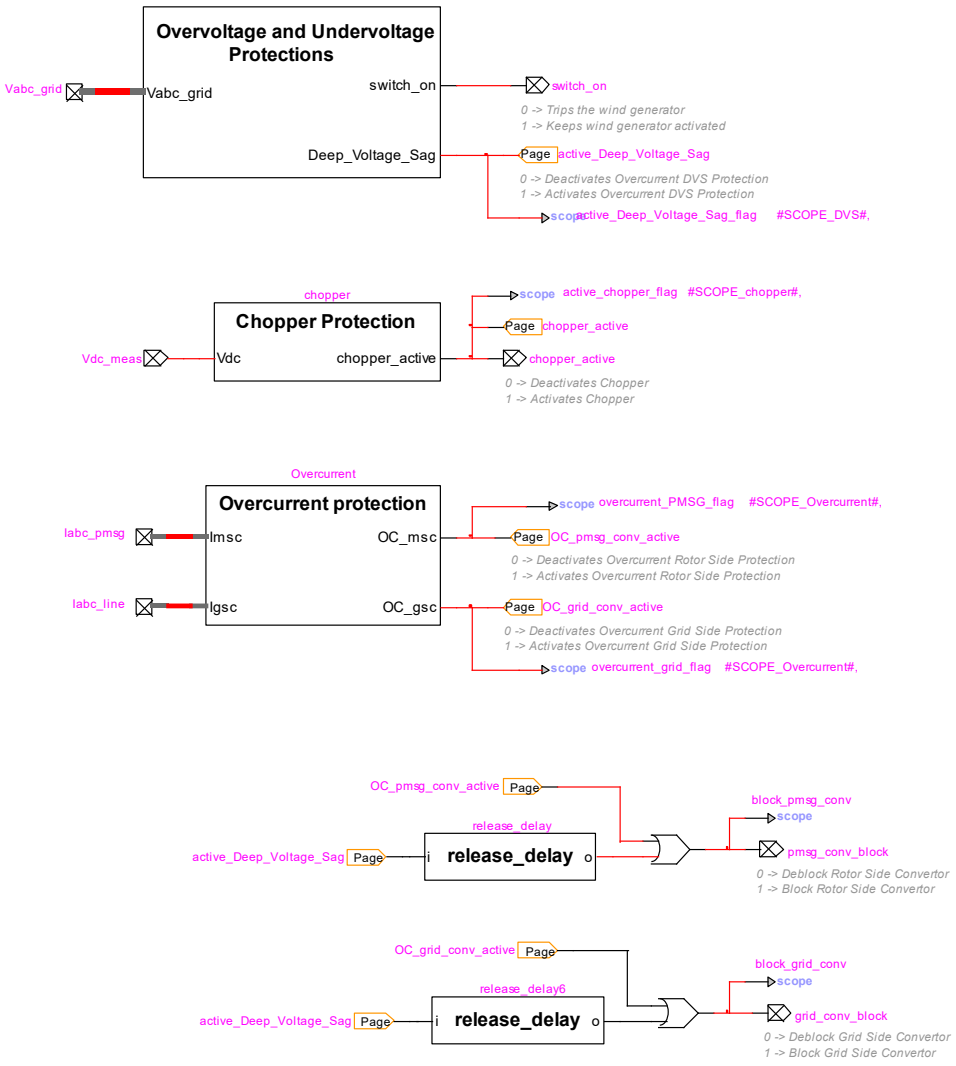

Figure 31 EMTP® diagram of protection system block

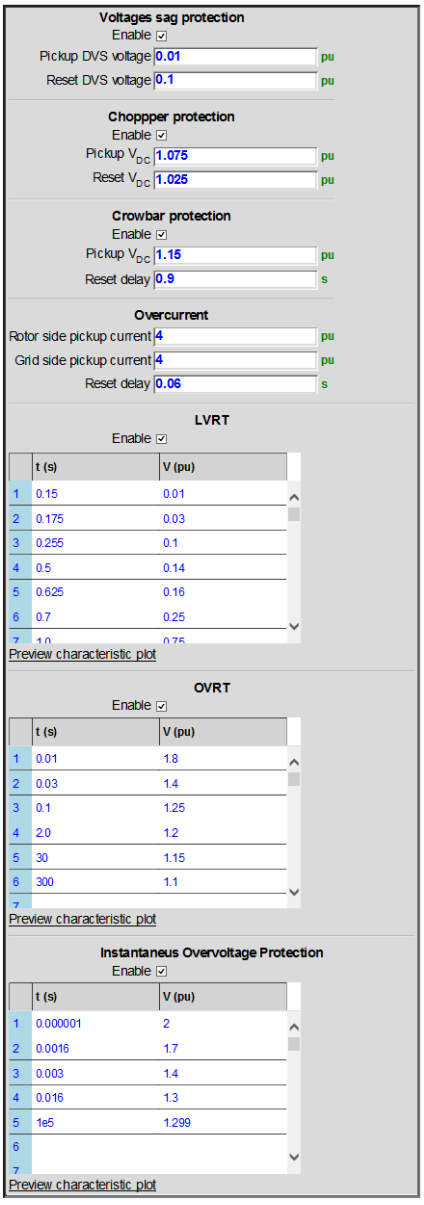

Figure 32 Protection system parameters

3.2.4.1 Overvoltage and Undervoltage protections

Figure 33 shows overvoltage and undervoltage protections. It includes rms-based over/under voltage relays, cumulative instantaneous overvoltage relays, deep voltage sag detectors.

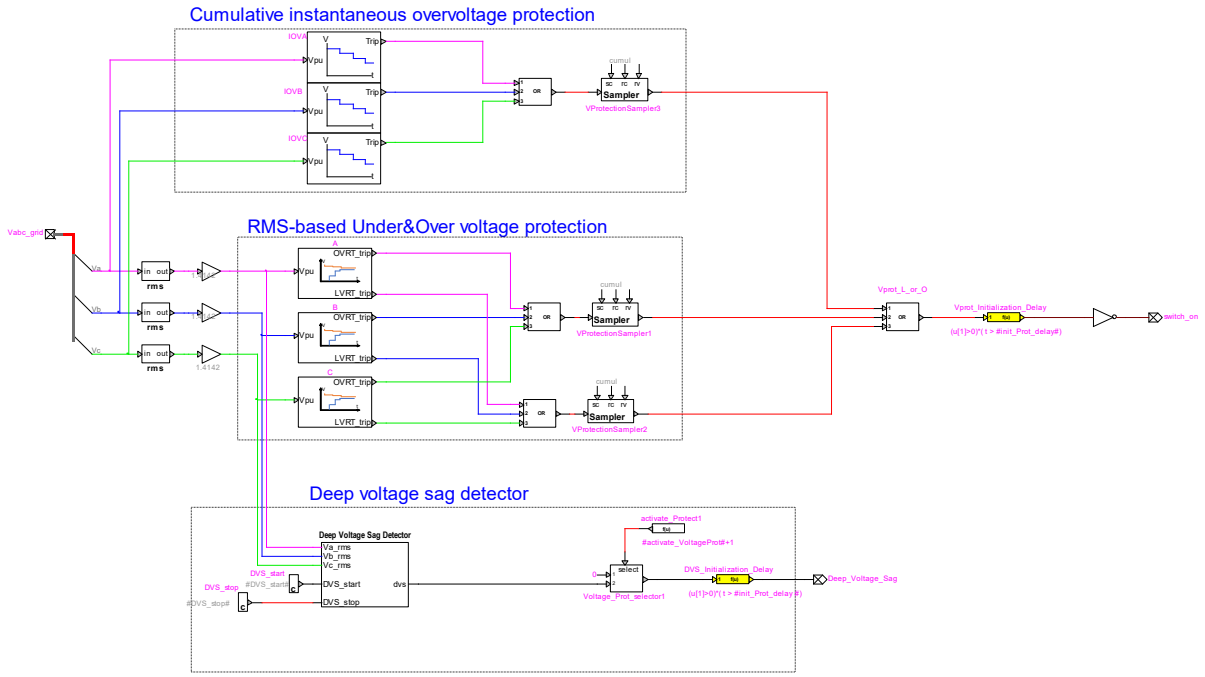

Figure 33 EMTP® diagram of overvoltage and undervoltage protections

The instantaneous over voltage protection suggested by IEEE Std 1547-2018 is developed and added to the protection schemes. This protection works based on a cumulative instantaneous overvoltage. Figure 34 shows the threshold values of the voltage (per unit of nominal instantaneous peak base) and cumulative duration of the transient overvoltage protection, and they can be modified in the device mask. The cumulative duration is the sum of durations when the instantaneous voltage exceeds the protection threshold over a one-minute time window.

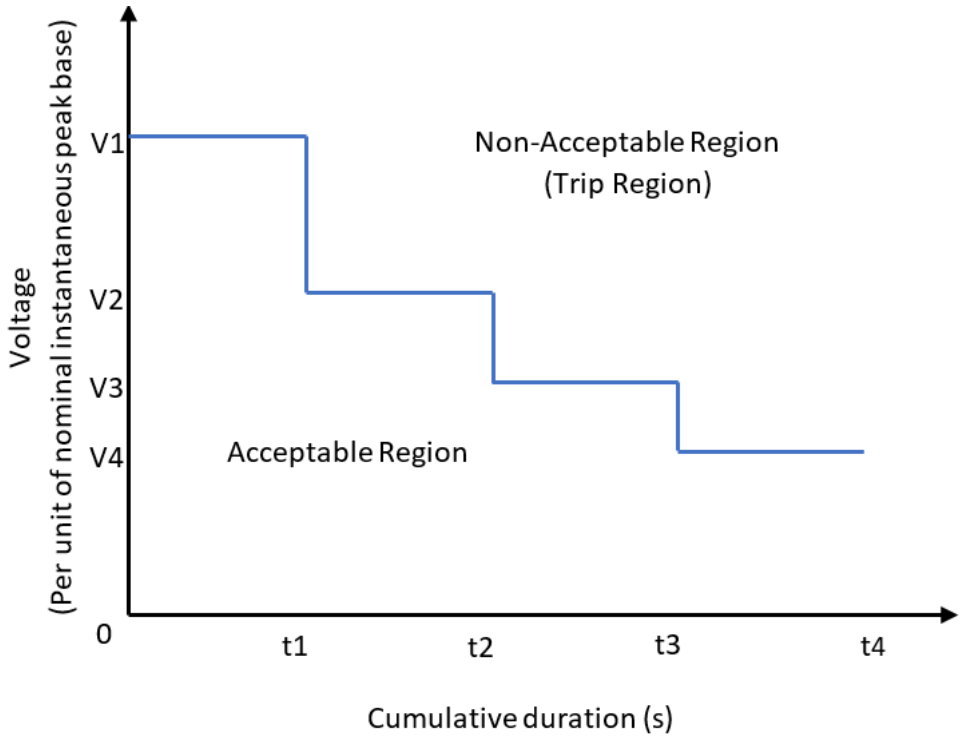

Figure 34 Transient overvoltage limits

The rms-based over/under voltage protections are designed based on the technical requirements set by Hydro Quebec for the integration of renewable generation. The over/under voltage limits as a function of time are presented in Figure 35 and can be modified in the device mask. The voltages below the red line reference and above the black line reference correspond to the ride-through region where the park is supposed to remain connected to the grid. This block measures the rms voltages on each phase and sends a trip signal to the inverter circuit breaker when any of the phase rms voltage violates the limits in Figure 35.

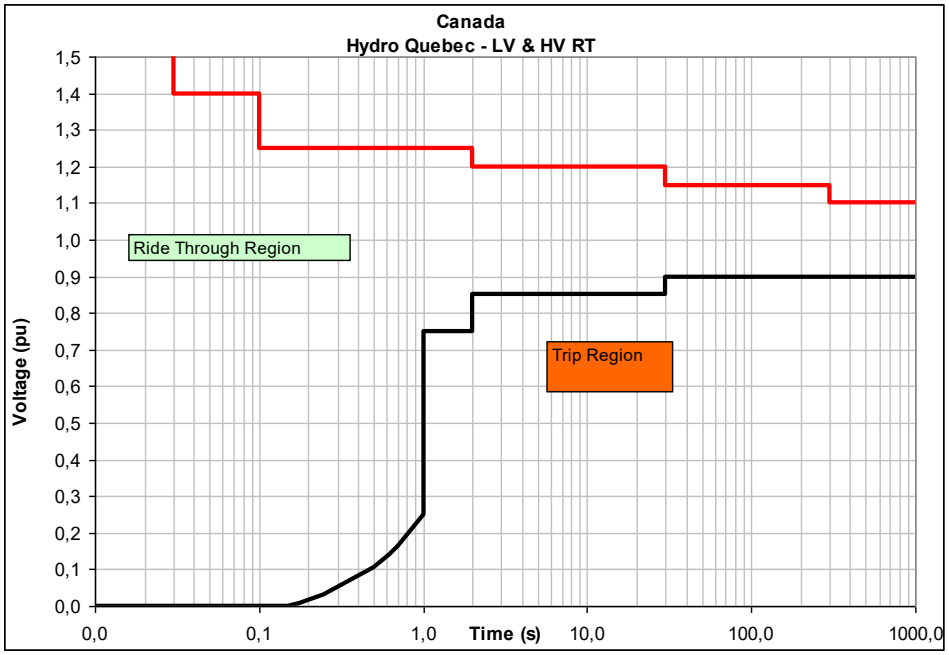

Figure 35 LVRT and HVRT requirements [16]

The “Deep Voltage Sag Detector” block temporary blocks the GSC and MSC in order to prevent potential overcurrents and restrict the FRT operation to the faults that occur outside the wind farm.

3.2.4.2 dc Overvoltage Protection Block

The function of dc chopper is to limit the dc bus voltage. It is activated when the dc bus voltage exceeds $|U_{chopper-ON}|$ and deactivated when dc bus reduces below $|U_{chopper-OFF}|$. The EMTP diagram of the “dc overvoltage protection” is shown in Figure 36.

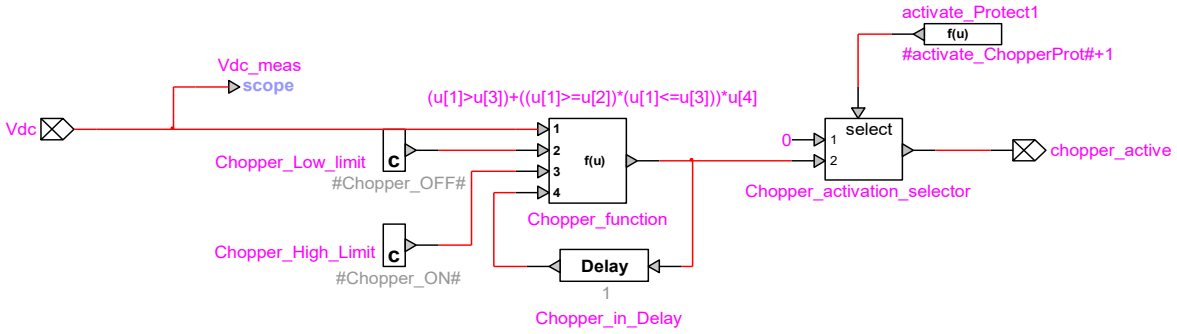

Figure 36 EMTP® diagram of dc overvoltage protection block

3.2.4.3 Overcurrent Protection Block

The overcurrent protection shown in Figure 37 blocks the converter temporarily when the converter current exceeds the pre-specified limit.

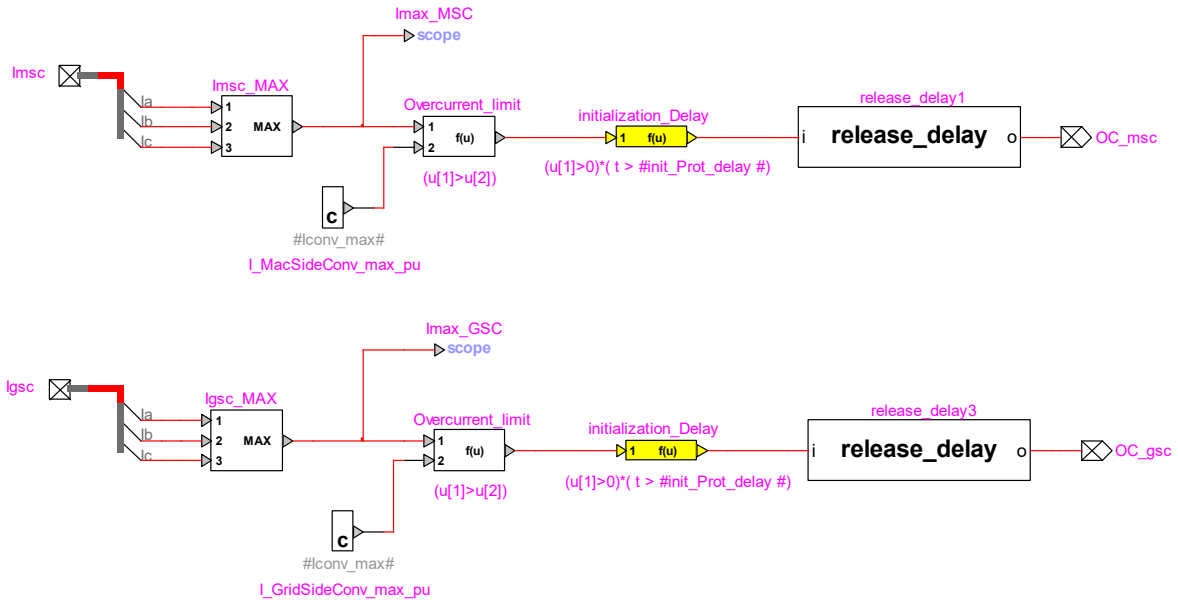

Figure 37 EMTP® diagram of overcurrent protection block

3.3 DFIG based Wind Park Model in EMTP®

The EMTP diagram of the DFIG based Wind Park is shown in Figure 38. It is composed of “Wind Turbine”, “WT Electrical System”, “WT Control System”, “WP Control System” blocks, PI circuit that represents equivalent collector grid, wind park transformer and initialization source with load flow constraint.

This model is the same as with the FSC based wind park model except “WT Electrical System” and “WT Control System” blocks.

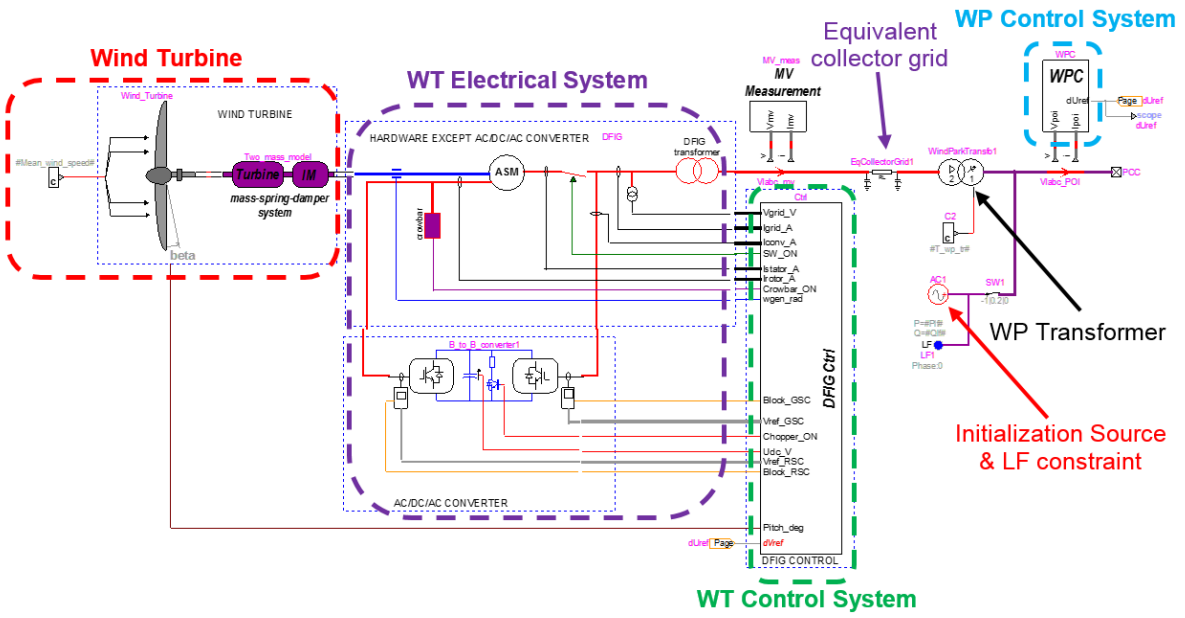

Figure 38 EMTP® diagram of the DFIG based Wind Park

3.3.1 DFIG Wind Turbine Electrical System Block

The EMTP diagram of the "WT Electrical System" block consists of IG, ac-dc-ac converter system, GSC choke filter, shunt ac harmonic filters, crowbar and WT transformer as shown in Figure 39.

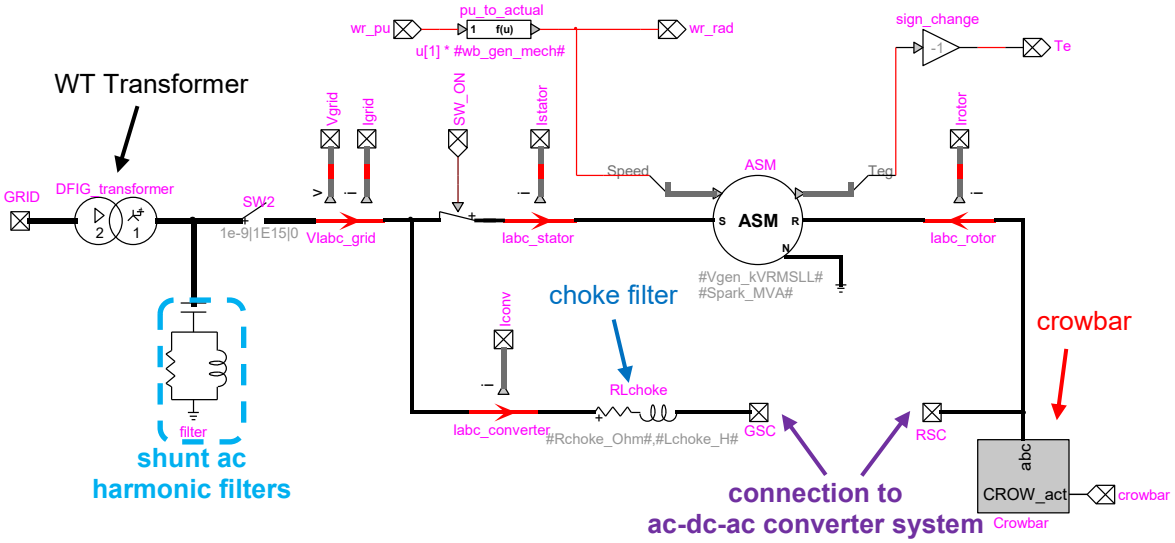

Figure 39 EMTP® diagram of DFIG "WT Electrical System" block

The measurement blocks are used for monitoring and control purposes. The monitored variables are IG stator, IG rotor, GSC and total DFIG currents, and DFIG terminal voltages. The dc voltage is also monitored (in ac-dc-ac converter system block) as well as the IG electromagnetic torque. All variables are monitored as instantaneous values and meter locations and directions are shown in Figure 39. The ac-dc-ac converter system block details have been presented in Section 3.1.

Similar to the FSC WT, the "shunt ac harmonic filters" block includes two band-pass filters as shown in Figure 21. These filters are tuned at switching frequencies harmonics n_1 and n_2 of the GSC.

3.3.2 DFIG Wind Turbine Control System Block

The EMTP diagram of the DFIG WT control system block is shown in Figure 40. The sampled signals are converted to pu and filtered. The sampling frequency are set to to 22.5 kHz and 11.25 kHz (from device mask as shown in Figure 12) for GSC and RSC, respectively. The “sampling” blocks are deactivated in AVM due to large simulation time step usage. In the generic model, 4th order Bessel type low pass filters are used. The cut-off frequencies of the filters are set to 4.5 kHz and 2.25 kHz for GSC and RSC, respectively. However, the order (up to 8th order), the type (Bessel and Butterworth) and the cut-off frequencies of the low pass filters can be modified from device mask as shown in Figure 12. The “RSC Compute Variables” and “GSC Compute Variables” blocks do the dq transformation required for the vector control. The RSC control (“Rotor Control” block) operates in the stator flux reference frame and the GSC (“Grid Control” block) operates in the stator voltage reference frame. The pitch control is activated when the wind speed increases above the rated value and given in Figure 4. The protection block includes the over/under voltage relay, the deep voltage sag detector, the dc chopper control, the crowbar protection and overcurrent detector.

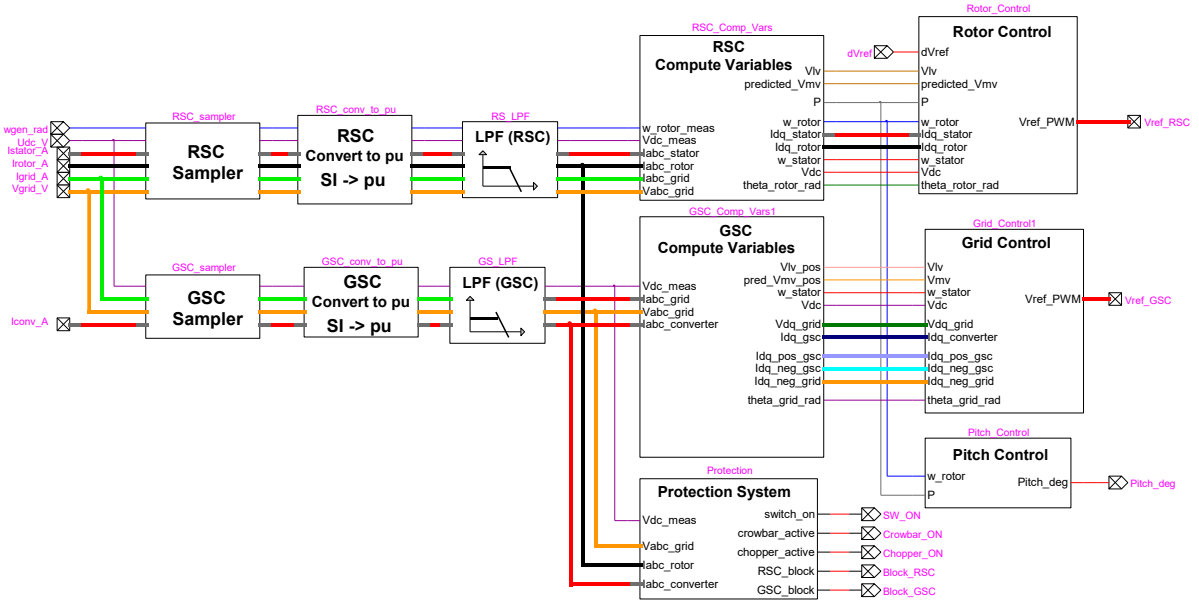

Figure 40 EMTP® diagram of DFIG “WT Control System” block

The direct axis d is aligned with the stator voltage in transformation matrix (see (19)); therefore, the rotor and stator currents are shifted to align with the stator flux. The shifted-angle flux block used to achieve a Stator Flux Orientation (SFO) is shown in Figure 41.

The frequency of the rotor voltage is controlled so that under steady conditions, the combined speed of the rotor plus the rotational speed of the rotor flux vector matches that of the synchronously rotating stator flux vector fixed by the network frequency. Manipulation of the rotor voltage permits control of the generator operating conditions.

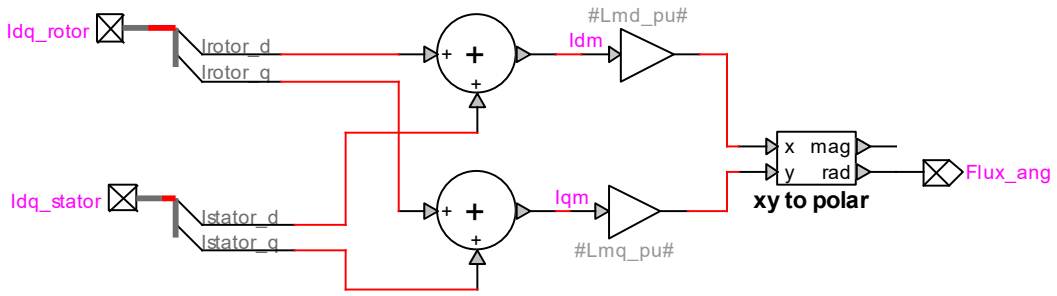

Figure 41 EMTP® diagram of Flux angle calculation

3.3.2.1 DFIG Rotor Side Converter Control

The EMTP diagram of the "Rotor Control" block is shown in Figure 42. The d- and q-axis currents of RSC (i_{dr} and i_{qr} in Figure 10) are used to control the positive sequence voltage at MV side of DFIG transformer (V_{wt}^{+}) and the active power output of DFIG. The positive sequence voltage at MV side of DFIG WT transformer is not directly measured by the WT controller and it is approximated using (31) - (33).

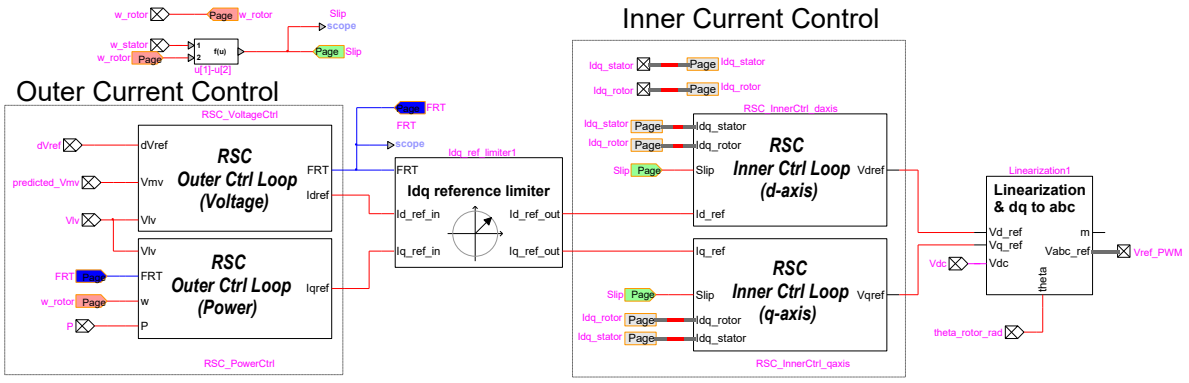

Figure 42 EMTP® diagram of DFIG "Rotor Control" block

The d-axis reference current is calculated by the proportional outer voltage control

$$i'_{dr} = K_V\left(V' - V_{wt}^{+}\right) + i_{dr-m} \tag{50}$$

In (50) i_{dr-m} is the compensating term for the reactive current absorbed by the IG and approximated by

$$i_{dr-m} = \tilde{V}_{wt}^{+} / (\omega_s L_m) \tag{51}$$

where L_m is the IG magnetizing inductance and $\tilde{V}_{wt}^{+}$ is the positive sequence voltage at DFIG WT terminals.

The q-axis reference current is calculated by the power controller

$$i'_{qr} = \left(K_{PP} + K_{IP}/s\right)\left(P' - P\right) \tag{52}$$

During normal operation, the controller gives the priority to the active currents.

$$
\begin{aligned}
i'_{qr} &< I_{qr}^{lim} \\
i'_{dr} &< I_{dr}^{lim} = \sqrt{\left(I_r^{lim}\right)^2 - \left(i'_{qr}\right)^2}
\end{aligned}
\tag{53}
$$

where I_{dr}^{lim}, I_{qr}^{lim} and I_r^{lim} are the limits for d-axis, q-axis and total RSC currents, respectively.

When the FRT function is activate, the RSC controller gives the priority to the reactive current by reversing the d- and q-axis current limits given in (53).

The RSC inner control loop is designed based on the IMC method [12][17] considering the Γ representation of the IG [17] shown in Figure 43. The Γ representation eliminates the complexity of the well-known T representation without loss of information or accuracy. It is obtained by adjusting the rotor/stator turn ratio for eliminating the stator leakage inductance. The Γ representation parameters are as follows:

$$\gamma = L_s / L_m \tag{54}$$

$$L_M = L_s = \gamma L_m \tag{55}$$

$$L_\sigma = \gamma L_{ls} + \gamma^2 L_{lr} \tag{56}$$

$$R_R = \gamma^2 R_r \tag{57}$$

where L_m is the magnetizing inductance, L_{ls} and L_{lr} are the stator and rotor leakage inductances, and R_s and R_r are the stator and rotor resistances of the machine.

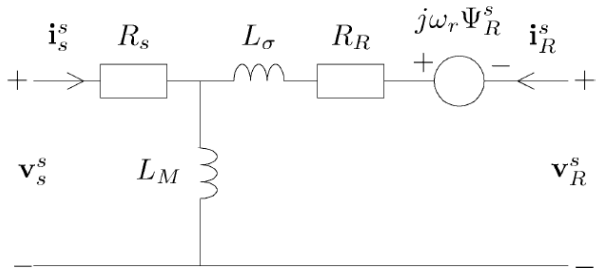

Figure 43 Γ representation of induction machine

After transformation, the rotor currents, fluxes and voltages become

$$\mathbf{i_R} = \mathbf{i_r} / \gamma \tag{58}$$

$$\boldsymbol{\lambda_R} = \gamma\, \boldsymbol{\lambda_r} \tag{59}$$

$$\mathbf{v_R} = \gamma\, \mathbf{v_r} \tag{60}$$

By neglecting $d\boldsymbol{\lambda_s}/dt$ [18], the rotor side voltages can be written as:

$$v_{dR} = R_R\, i_{dR} + L_\sigma \frac{d\, i_{dR}}{dt} - \omega_r\, L_\sigma\, i_{qR} \tag{61}$$

$$v_{qR} = R_R\, i_{qR} + L_\sigma \frac{d\, i_{qR}}{dt} - \omega_r \left[(L_M + L_\sigma)\, i_{dR} + L_M i_{ds}\right] \tag{62}$$

The i_{dR} and i_{qR} errors are processed by the PI controller to give v_{dR} and v_{qR}, respectively. To ensure good tracking, feed-forward compensating terms for $-\omega_r\, L_\sigma\, i_{qR}$ in (61) and $\omega_r \left[(L_M + L_\sigma)\, i_{dR} + L_M i_{ds}\right]$ in (62) are added. The converter reference voltages become

$$v'_{dR} = \left(k_p + k_i/s\right)\left(i'_{dR} - i_{dR}\right) - \omega_r\, L_\sigma\, i_{qR} \tag{63}$$

$$v'_{qR} = \left(k_p + k_i/s\right)\left(i'_{qR} - i_{qR}\right) - \omega_r\left[\left(L_M + L_\sigma\right) i_{dR} + L_M i_{ds}\right] \tag{64}$$

Using (25) with

$$G_{rsc}(s) = 1/\left(R_R + sL_\sigma\right) \tag{65}$$

the PI controller parameters of the inner current control loop are found as

$$k_p = \alpha_c L_\sigma \tag{66}$$

$$k_i = \alpha_c R_R \tag{67}$$

The PI controller parameters are calculated for the RSC rise time given in the device mask as shown in Figure 12.

The RSC inner current control has variable conversion blocks for the input RSC currents and the output RSC voltages as shown in Figure 44.

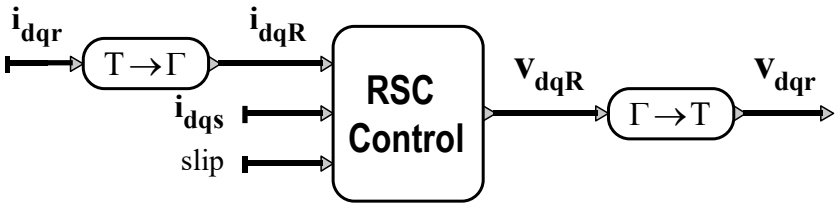

Figure 44 Conversion at RSC input and output variables

3.3.2.2 GSC Grid Side Converter Control

The function of GSC is maintaining the dc bus voltage V_{dc} at its nominal value. It operates at unity power factor except severe fault conditions. The EMTP diagram of the "Grid Control" block is shown in Figure **45**. GSC control offers both coupled and decoupled sequence control options. User can select the GSC control option from the device mask as shown in Figure 12.

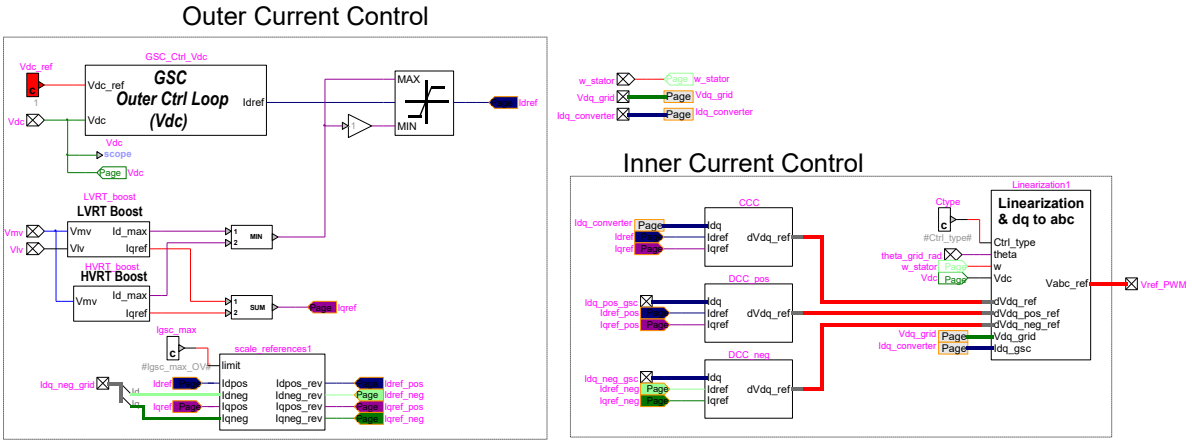

Figure 45 **EMTP® diagram of DFIG "Grid Control" block**

3.3.2.2.1 DFIG GSC Coupled Control

Except the q-axis reference current calculation, the DFIG WT GSC control is similar to the FSC WT GSC control. In DFIG WTs, the GSC operates at unity power factor, hence the q-axis reference current is set to zero (i.e. $i'_{qg} = 0$). However, GSC starts injecting reactive currents during faults when the RSC reactive current contribution is not sufficient to satisfy the grid code requirement due to the reactive current absorbed by the IG. In that condition GSC q-axis reference current becomes

$$i'_{qr} = K_V\left(V' - V^{+}_{wt}\right) - \left(I^{lim}_{dr} - i_{dr-m}\right) \qquad (68)$$

Similar to RSC, the priority is given to the GSC reactive currents when FRT function is activate. In order to improve the high voltage ride through (HVRT) capability of the DFIG WT, reactive current contribution of GSC is also used. The GSC reactive current contribution is achieved by “LVRT boost” and “HVRT boost” blocks (shown in Figure 46 and Figure 47, respectively) during low voltage and high voltage conditions.

The PI controller parameters are calculated for the GSC rise time given in the device mask as shown in Figure 12. The parameters regarding GSC reactive current contribution can be modified from the device mask as shown in Figure 12.

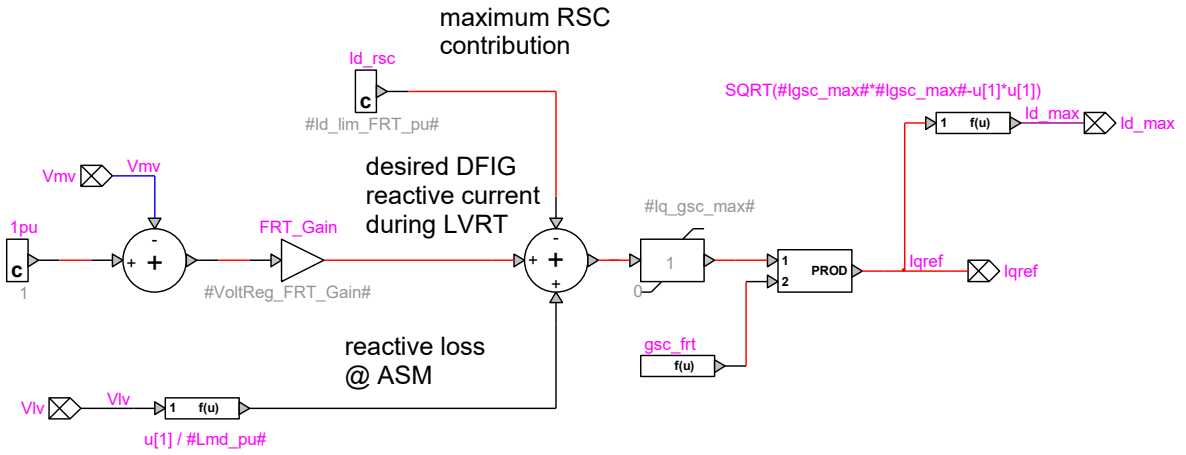

Figure 46 EMTP® diagram of “LVRT boost” block

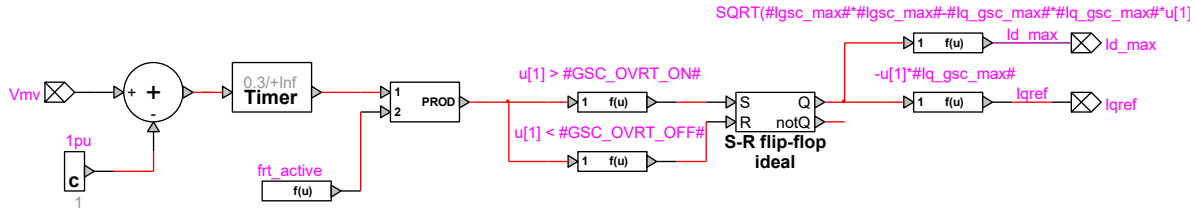

Figure 47 EMTP® diagram of “HVRT boost” block

3.3.2.2.2 DFIG Side Converter Decoupled Sequence Control

Unbalanced steady state operation and fault conditions give rise to high frequency components in rotor currents and torque pulsations [19]. To mitigate the corresponding stress different control methods has been proposed [20] - [24]. The primary objective in these methods is to reduce the oscillating air gap torque during periods of asymmetry so that the drive-train of the wind turbine is not subjected to the resulting stress. Either RSC or GSC (or both of them) can be used for this purpose. The performance of these methods depends on the severity of the voltage dip at DFIG terminal as well as the severity of

its asymmetry. The major limiting factor of the performances of these methods is the FRT requirement specified by the grid code.

The implementation in this document considers the method in which the GSC compensates the negative sequence current required in the network during any unbalanced operation [23]. As the GSC will supply the negative sequence components for the currents to the grid, the stator currents will remain balanced as shown in Figure 48.

The reference GSC currents ($i_{dg}^{+\prime}, i_{qg}^{+\prime}, i_{dg}^{-\prime}, i_{qg}^{-\prime}$) will become

$$i_{dg}^{+\prime} = i_{dg}^{\prime}, \quad i_{qg}^{+\prime} = i_{qg}^{\prime}, \quad i_{dg}^{-\prime} = i_{dwt}^{-}, \quad i_{qg}^{-\prime} = i_{qwt}^{-} \tag{69}$$

The calculated reference values in (69) is revised considering the converter limit I_g^{lim}. For example when $\sqrt{\left(i_{dg}^{+\prime} + i_{dg}^{-\prime}\right)^2 + \left(i_{qg}^{+\prime} + i_{qg}^{-\prime}\right)^2} > I_g^{lim}$, the q-axis positive sequence current reference is revised as below

$$i_{qg}^{+\prime\prime} = i_{qg}^{+\prime}\left[I_g^{lim} \Big/ \sqrt{\left(i_{dg}^{+\prime} + i_{dg}^{-\prime}\right)^2 + \left(i_{qg}^{+\prime} + i_{qg}^{-\prime}\right)^2}\right] \tag{70}$$

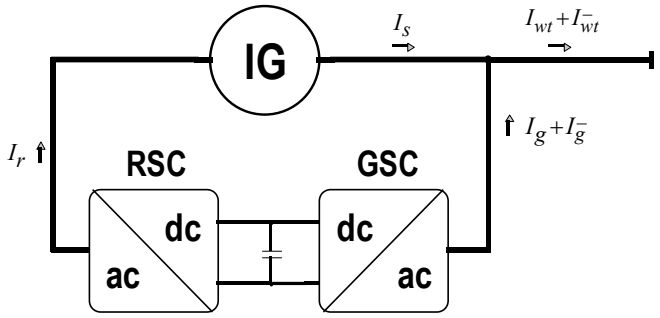

Figure 48 Negative sequence compensation through GSC

4 WIND PARK RESPONSE TO UNBALANCED FAULTS

This section provides a comparison between the wind park responses with coupled and decoupled sequence controls. Although the comparison is conducted for various type unbalanced faults in the 120 kV, 60 Hz test system shown in Figure 49 [25]-[27], only the 250 ms double line to ground (DLG) fault simulation scenarios are presented. The simulation scenarios are presented in Table I. The WT converters are represented with their AVMs. The simulation time step is 10 μs.

In the test system, the loads are represented by equivalent impedances connected from bus to ground on each phase. The transmission lines are represented by constant parameter models and transformers with saturation. The equivalent parameters for the 34.5 kV equivalent feeders are calculated on the basis of active and reactive power losses in the feeder for the rated current flow from each of the WTs [28]. The aggregated model of 1.5 MW, 60 Hz DFIG wind turbines is used for 45 units. In all simulations, the WT is operating at full load with unity power factor (i.e. $Q_{POI} = 0$).

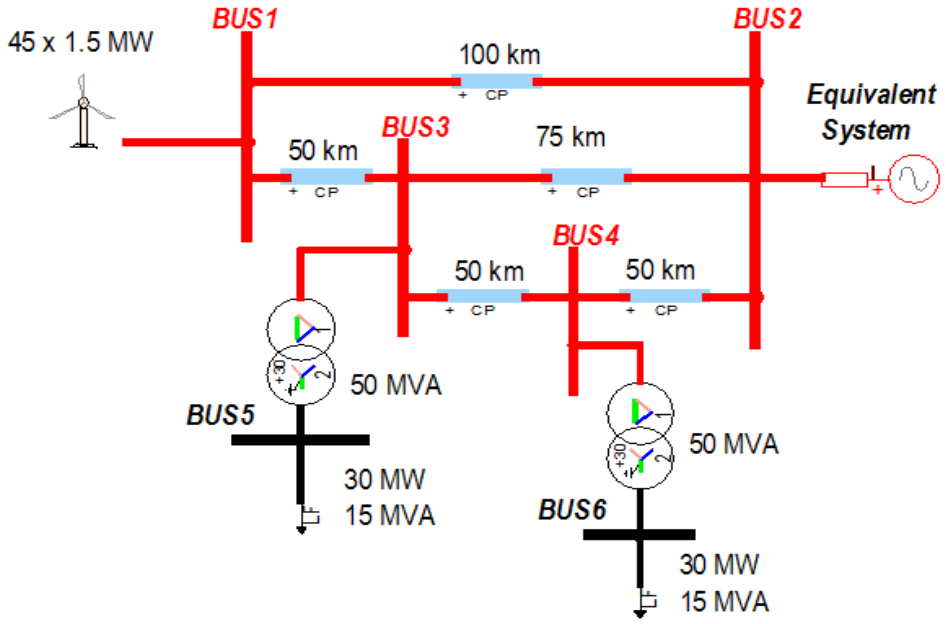

Figure 49 120 kV, 60 Hz test system

Table I Simulation Scenarios

Scenario	Fault Location	GSC Control Scheme
M1	BUS4	Coupled Control
M2	BUS4	Decoupled Sequence Control
N1	BUS6	Coupled Control
N2	BUS6	Decoupled Sequence Control

4.1 FSC based Wind Park Response to Unbalanced Faults

4.1.1 Simulation Scenarios M1 and M2 with FSC based Wind Park

As shown in Figure 50, the simulated unbalanced fault results second harmonic pulsations in the active power output of FSC WT in scenario M1. These second harmonic pulsations are eliminated in the scenario M2 with decoupled sequence control scheme in GSC at the expense of a reduction in the active power output of FSC WT as shown in Figure **51**. On the other hand, the reactive power output of FSC WT is similar in scenarios M1 and M2. This is due to the strict FRT requirement on positive sequence reactive currents.

The performance of the GSC decoupled sequence control is limited to the GSC rating as well as the FRT requirement specified by the grid code. The complete elimination of second harmonic pulsations cannot be achieved when the required GSC current output exceeds its rating. It should be noted that, when the electrical distance between the WP and unbalanced fault decreases, larger GSC currents are required to achieve both FRT requirement and the elimination of second harmonic pulsations.

The negative and positive sequence fault currents (I_n and I_p) of the WP in scenarios M1 and M2 are also quite different as illustrated in Figure 52. This difference strongly depends on the unbalanced fault type, its electrical distance to the WP, GSC rating and the FRT requirement specified by the grid code. It becomes less noticeable especially for the electrical distant faults such as an unbalanced fault at BUS6 as presented in Section 4.1.2.

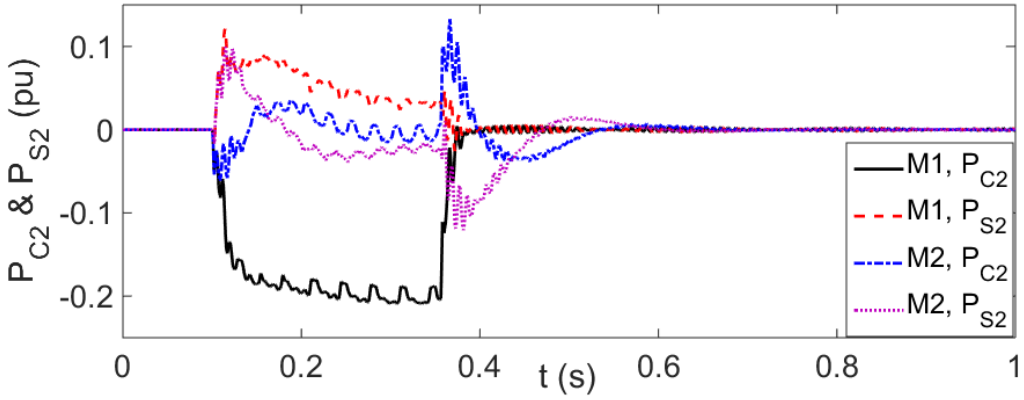

Figure 50 P_{C2} **and** P_{S2} **of aggregated FSC WT in scenarios M1 and M2**

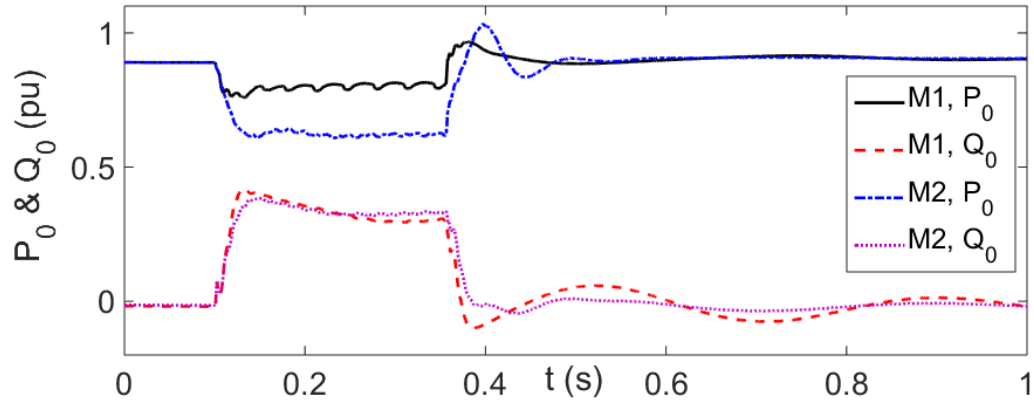

Figure 51 P_0 **and** P_0 **of aggregated FSC WT in scenarios M1 and M2**

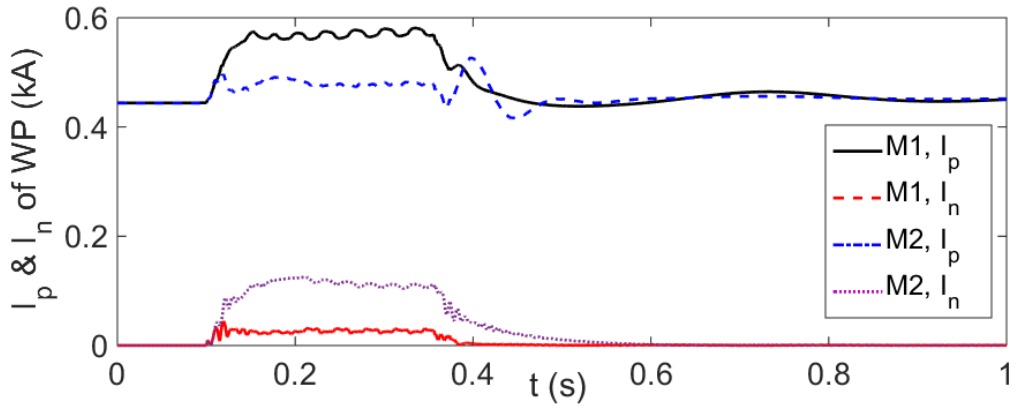

Figure 52 I_n and I_p of FSC WT based WP in scenarios M1 and M2

4.1.2 Simulation Scenarios N1 and N2 with FSC based Wind Park

As the electrical distance between the WP and the unbalanced fault is much larger in scenario N1 compared to scenario M1, both the voltage sag and the second harmonic pulsations in the active power output are much smaller in scenario N1 compared to the scenario M1 (see Figure 53 and Figure 50). As a result, the decupled sequence control of GSC achieves elimination of these pulsations in scenario N2 without any reduction in the active power output of FSC WT (see Figure 54 and Figure **51**). As seen from Figure 55 and Figure 52, the WP fault current contribution difference between the scenarios N1 and N2 also becomes less noticeable especially for positive sequence fault currents compared to the difference between scenarios M1 and M2.

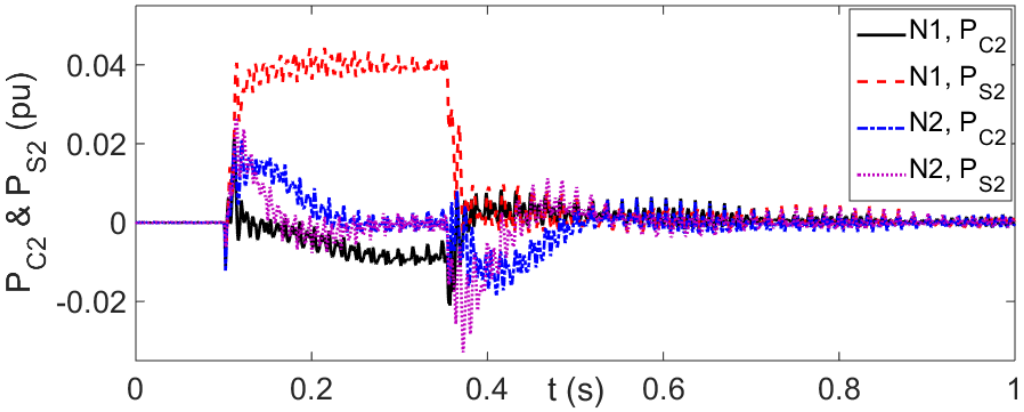

Figure 53 P_{C2} and P_{S2} of aggregated FSC WT in scenarios N1 and N2

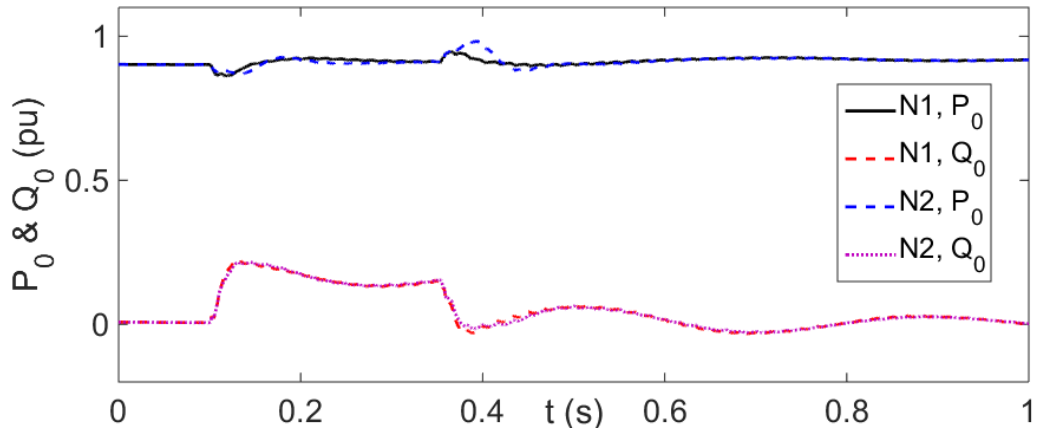

Figure 54 P_0 and Q_0 of aggregated FSC WT in scenarios N1 and N2

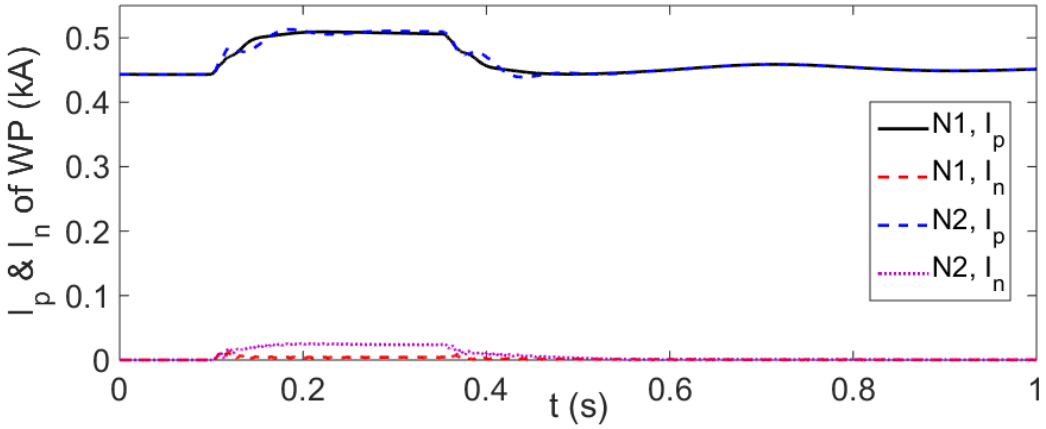

Figure 55 I_n and I_p of FSC WT based WP in scenarios N1 and N2

4.2 DFIG based Wind Park Response to Unbalanced Faults

4.2.1 Simulation Scenarios M1 and M2 with DFIG based Wind Park

As shown in Figure 56, the decoupled sequence control reduces the second harmonic pulsations in IG electromechanical torque. It should be noted that, the performance of decoupled sequence control is limited with the size of the GSC and the FRT requirement specified by the grid code as well as the unbalanced fault type, its electrical distance to the WP. With a larger size GSC, these pulsations can be totally eliminated as shown in Figure 57.

As shown in Figure 58, the active and reactive power outputs of the DFIG WT are similar for both coupled and decoupled sequence control schemes in GSC. However, the decoupled sequence control scheme in GSC results much higher negative sequence fault current contribution of the WP as shown in Figure 59.

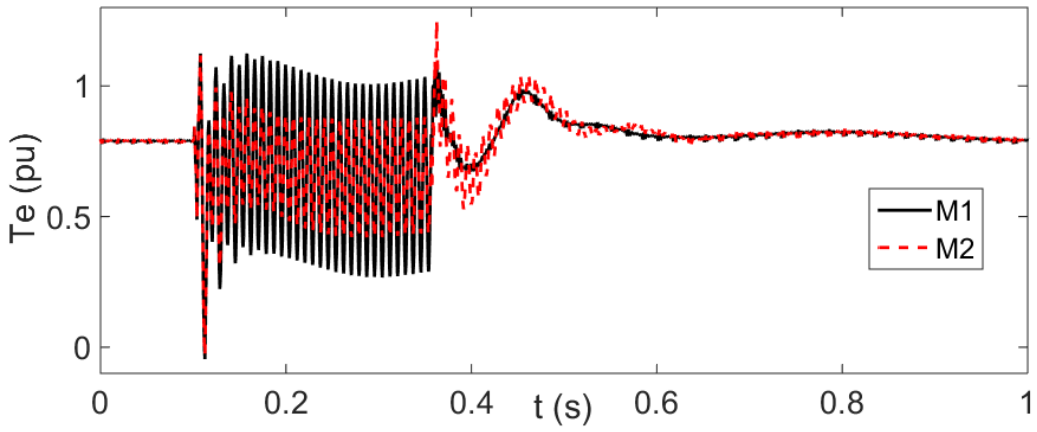

Figure 56 IG electromagnetic torque in scenarios M1 and M2

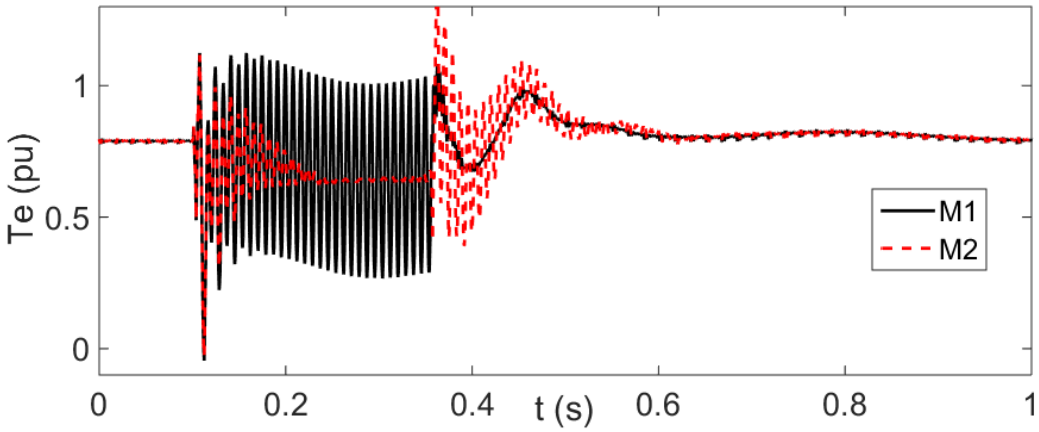

Figure 57 IG electromagnetic torque in scenarios M1 and M2 (with larger size GSC)

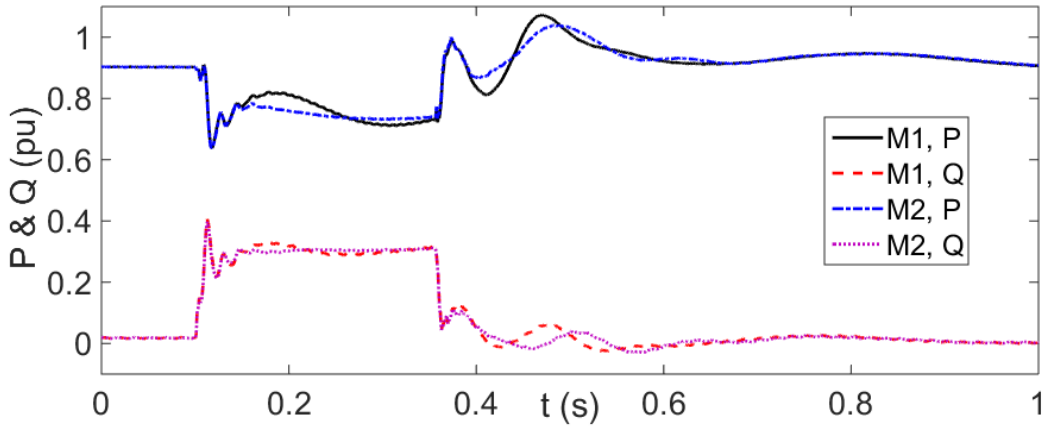

Figure 58 P and Q of aggregated DFIG WT in scenarios M1 and M2

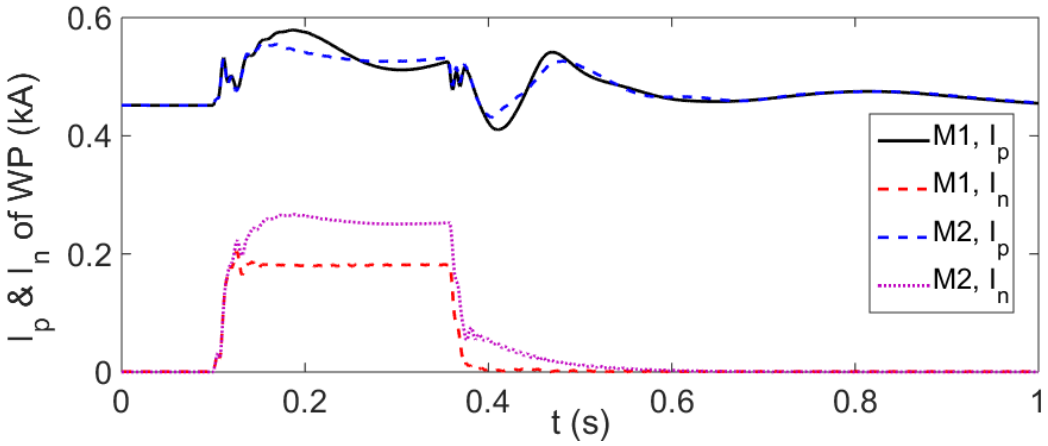

Figure 59 I_n and I_p of DFIG WT based WP in scenarios M1 and M2

4.2.2 Simulation Scenarios N1 and N2 with DFIG based Wind Park

As shown in Figure 60, decoupled sequence control totally eliminates the second harmonic pulsations in IG electromechanical torque. This is due to less severe voltage sag at POI due to large electrical distance between WP and the fault.

Similar to the BUS4 fault scenario, the active and reactive power output of DFIG WT is similar for both control schemes in GSC as shown in Figure 61.

Alike BUS4 fault scenario, the decoupled sequence control scheme in GSC results much higher negative sequence fault current contribution of the WP as shown in Figure 62.

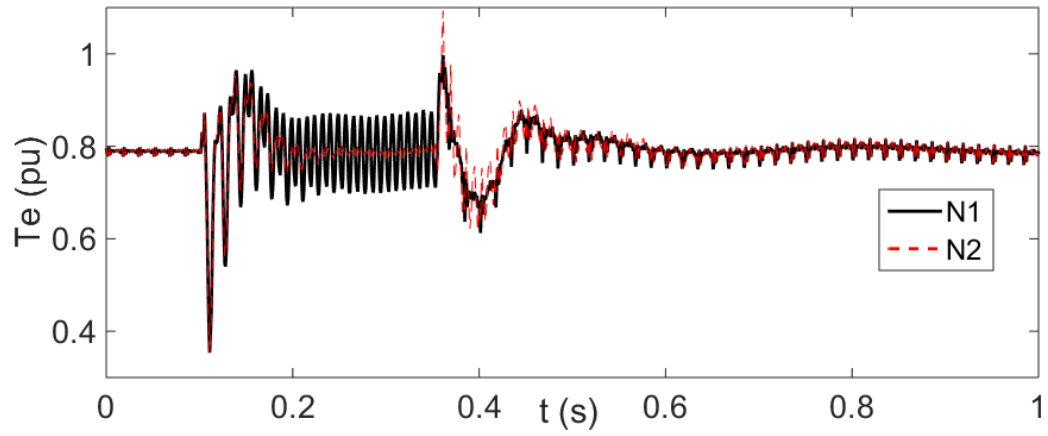

Figure 60 IG electromagnetic torque in scenarios N1 and N2

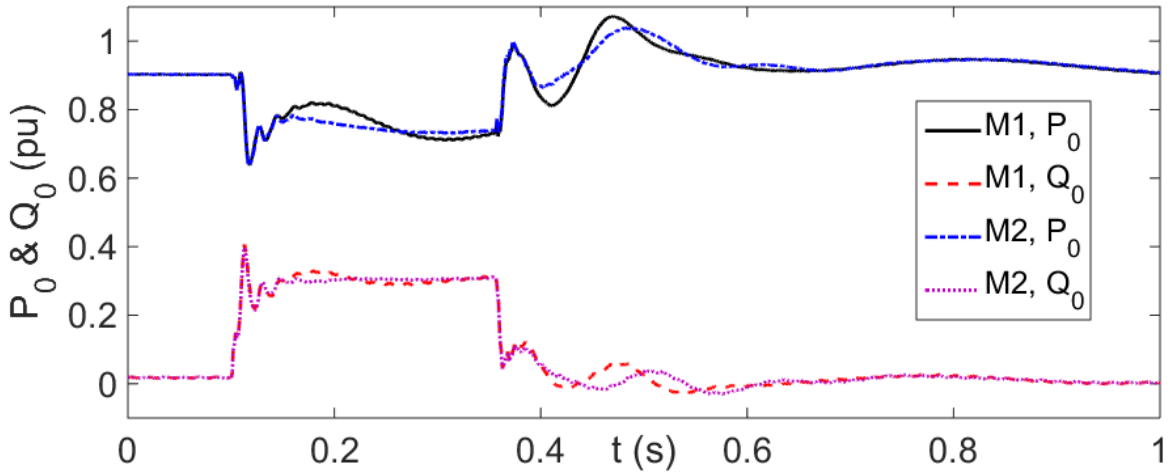

Figure 61 P and Q of aggregated DFIG WT in scenarios N1 and N2

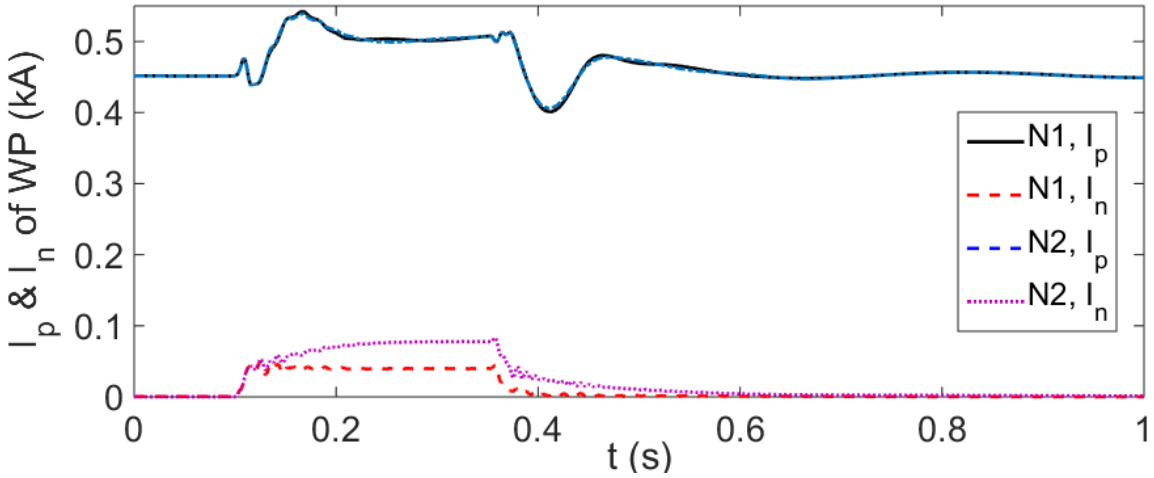

Figure 62 I_n and I_p of DFIG WT based WP in scenarios N1 and N2

5 AVERAGE VALUE MODEL PRECISION AND EFFICIENY

5.1 120 kV Test System Simulations

This section provides a comparison between average value model (AVM) and detailed model (DM) of the presented wind park models. The simulation scenario M2 in Table I is repeated for 50 µs simulation time step (M3) and for DM with 10 µs simulation time step (M4).

5.1.1 Simulation Scenarios M2 - M4 with FSC based Wind Park

As shown in Figure 63 - Figure 65, AVM usage instead of DM provides very accurate results even for 50 µs time step usage.

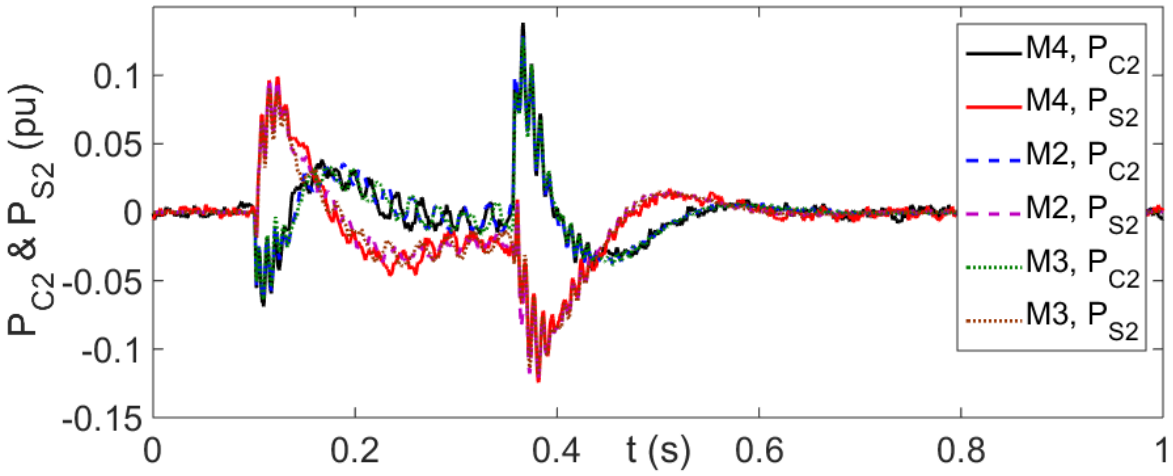

Figure 63 P_{C2} and P_{S2} of aggregated FSC WT in scenarios M2 - M4

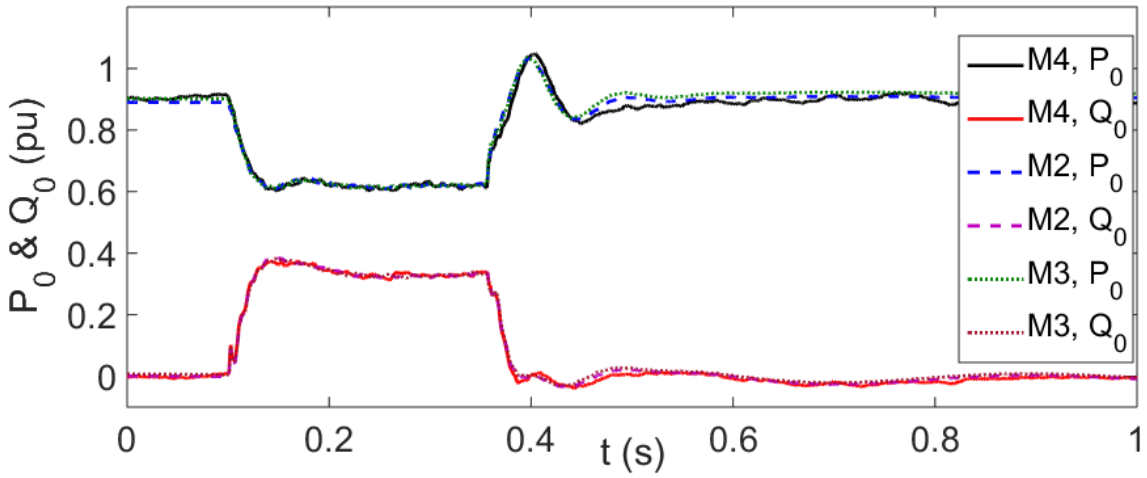

Figure 64 P_0 and Q_0 of aggregated FSC WT in scenarios M2 - M4

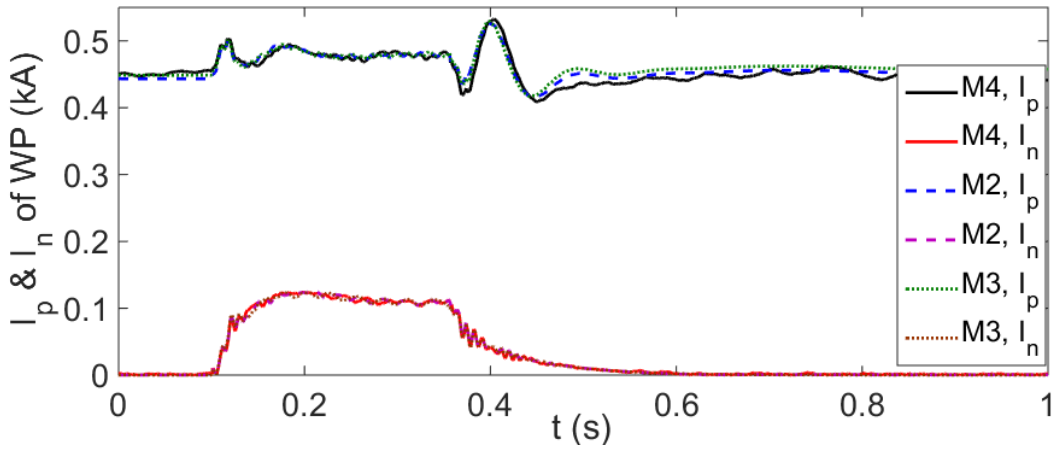

Figure 65 I_n and I_p of FSC WT based WP in scenarios M2 - M4

5.1.2 Simulation Scenarios M2 - M4 with DFIG based Wind Park

As shown in Figure 66 - Figure 68, AVM usage instead of DM provides acceptable accuracy even for 50 µs time step usage. From Figure 63 - Figure 68, it can be said that AVM provides more accurate results when it is used to represent FSC WT converters.

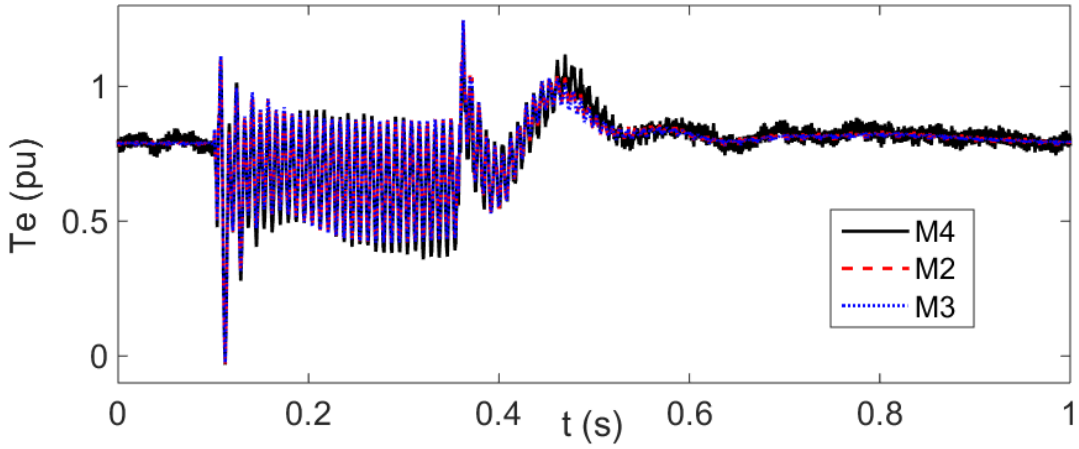

Figure 66 IG electromagnetic torque in scenarios in scenarios M2 - M4

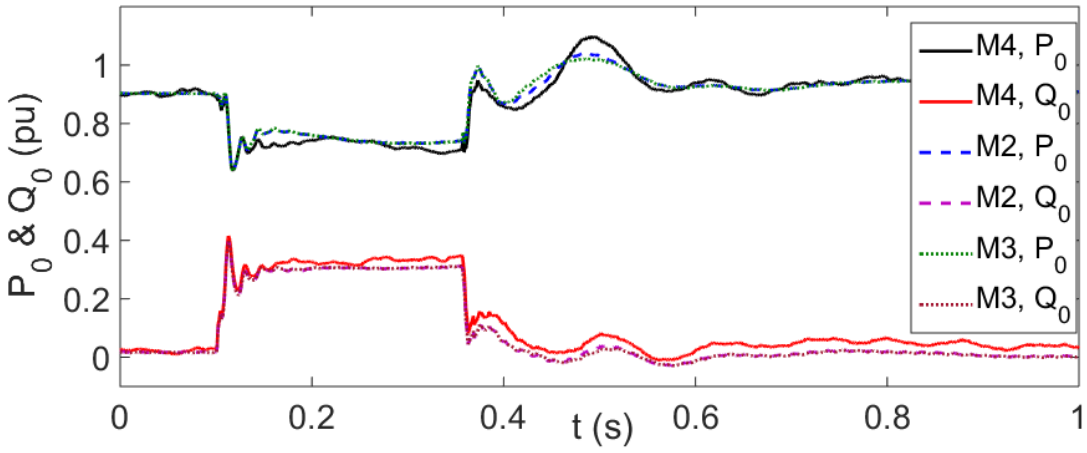

Figure 67 P_0 and Q_0 of aggregated DFIG WT in scenarios M2 - M4

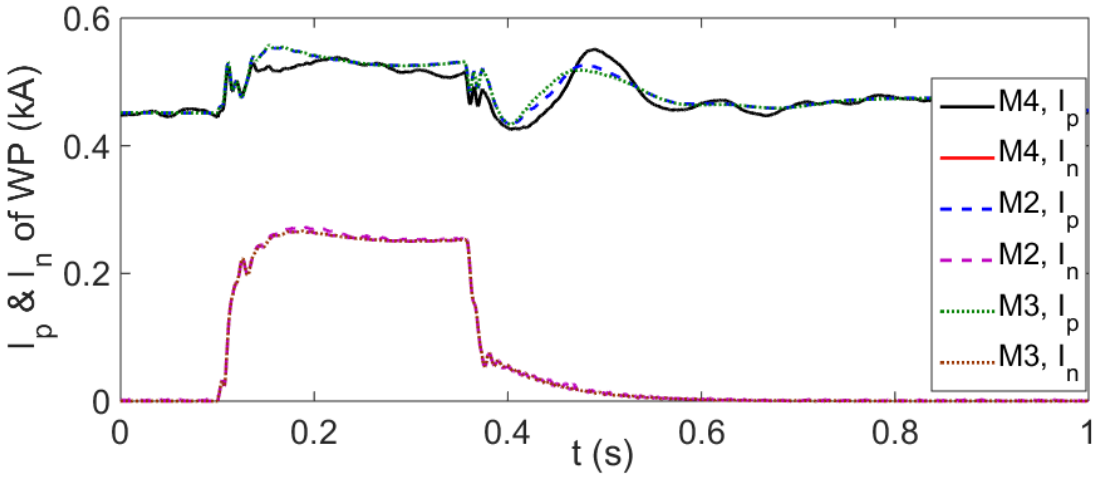

Figure 68 I_n and I_p of DFIG WT based WP in scenarios M2 - M4

5.2 IEEE 39 Bus System Simulations

A multi wind park system is developed from the IEEE-39 bus system by replacing two of the thermal power plants (TPPs), as shown in Figure 69. Both WPs have 400 MW (266 x 1.5 MW) installed capacity. However, the WP at bus B2 is FSC type and the WP at bus B25 is DFIG type. In the presented simulation the WPs are operating at full load (i.e. under nominal wind speed) with unity power factor (i.e. $Q_{POI} = 0$). The transmission lines are modeled with constant parameter models, and the saturation of transformers are taken into account.

In the simulated scenario, the disturbance is a DLG fault on transmission line that connects busses B3 and B4 (as bus B3 end). The fault is cleared with the operation of line circuit breakers indicated with CB1 and CB2 in Figure 69. The fault is applied at t = 1s. The fault clearing time is 200 ms (for testing purposes). The system is simulated for 3 s. The simulations are performed for the models and simulation time steps presented in Table II.

The presented waveforms in Figure 70 - Figure 75 demonstrate that AVM usage instead of DM provides acceptable accuracy even for 50 µs time step usage while providing a significant computational gain as illustrated in Table III. The computational gain over DM is more than 9 when the AVM is used with 50 µs time step.

Table II IEEE 39 Bus System Simulations

Scenario	WT Converter Model	Simulation Time Step
S1	DM	10 µs
S2	AVM	10 µs
S3	AVM	50 µs

Table III IEEE 39 Bus System Simulations CPU Timings

Scenario	CPU time
S1	1368 s
S2	615 s
S3	145 s

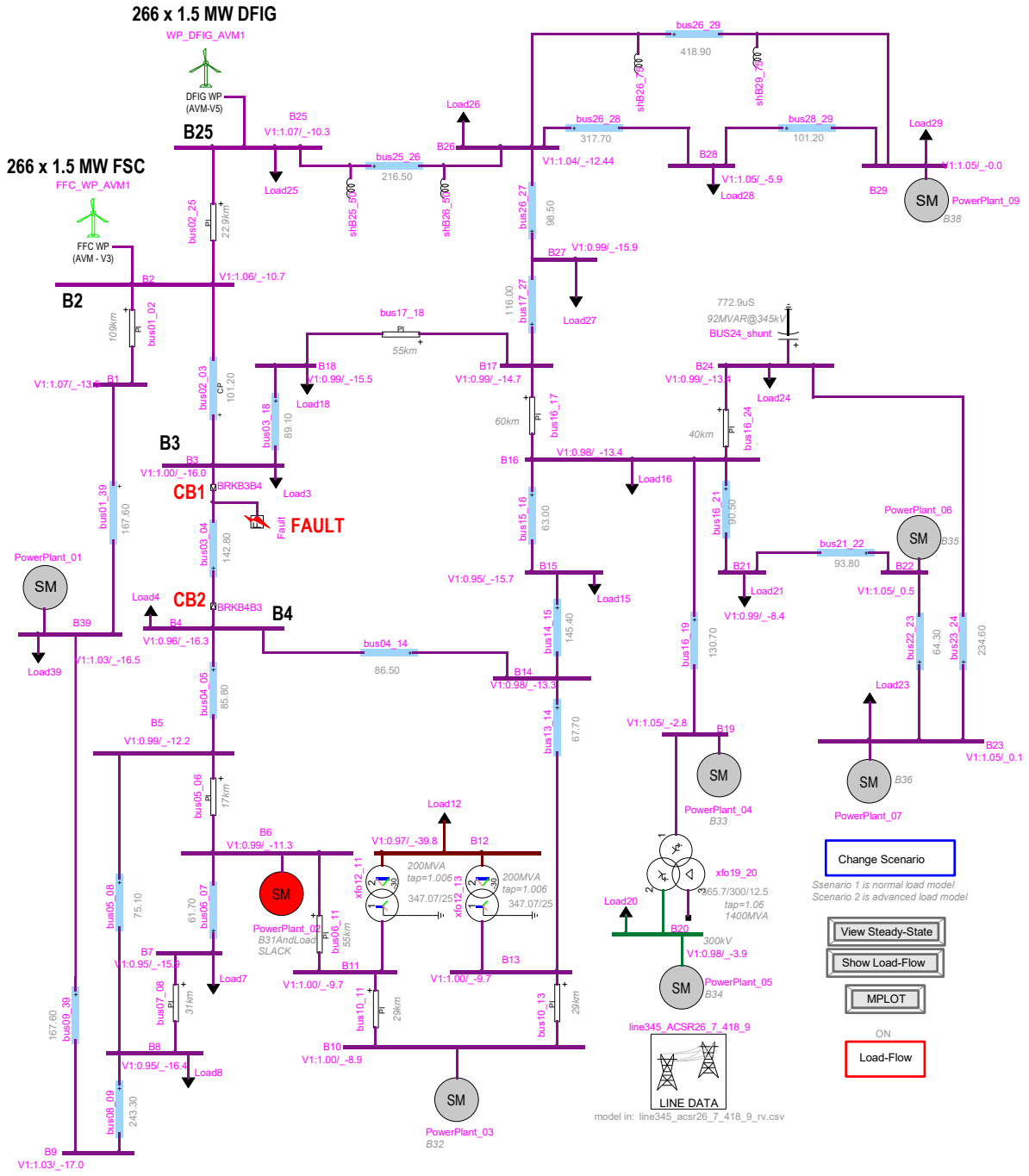

Figure 69 IEEE 39 Bus System with Wind Parks

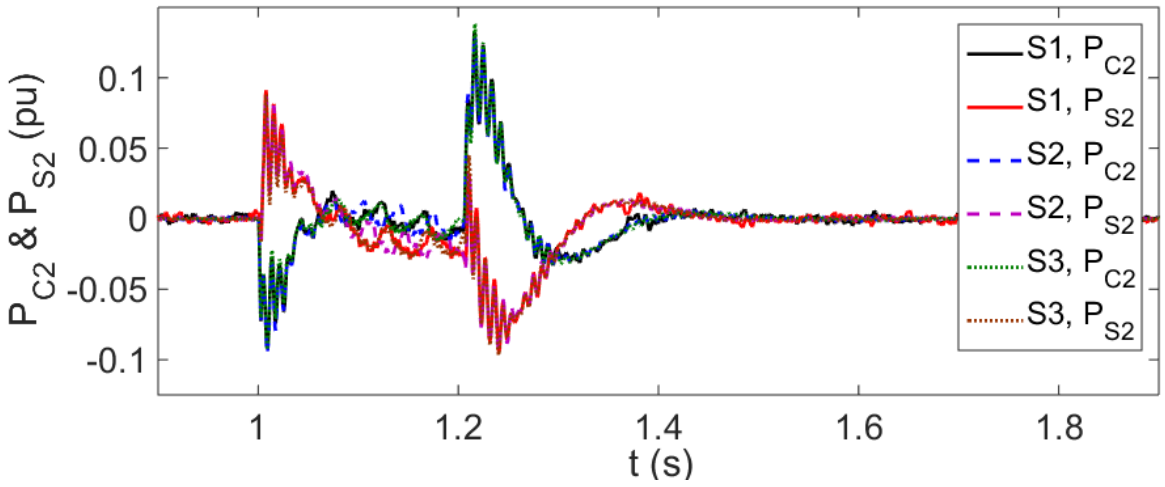

Figure 70 P_{C2} and P_{S2} of aggregated FSC WT in IEEE 39 bus system simulation

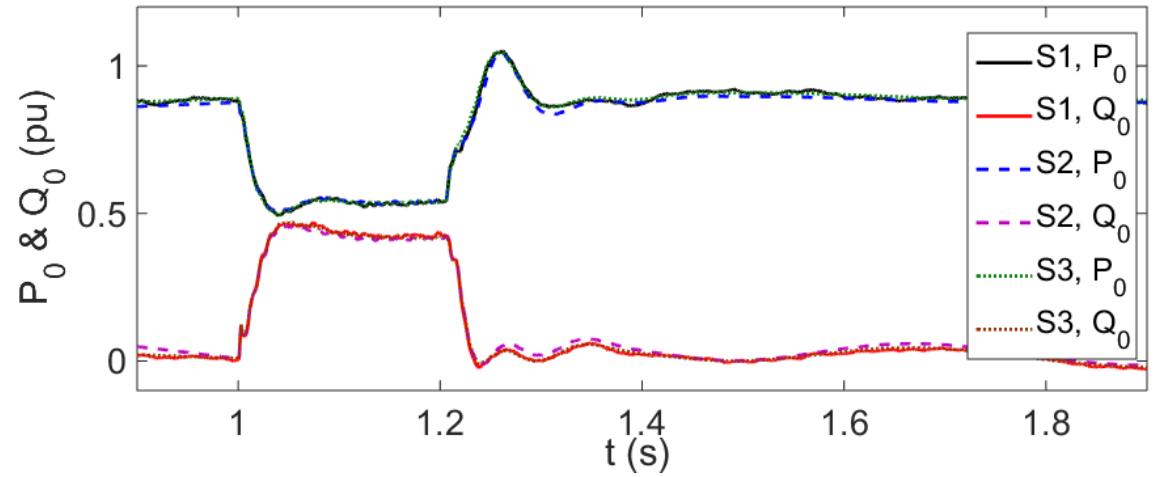

Figure 71 P_0 and Q_0 of aggregated FSC WT in IEEE 39 bus system simulation

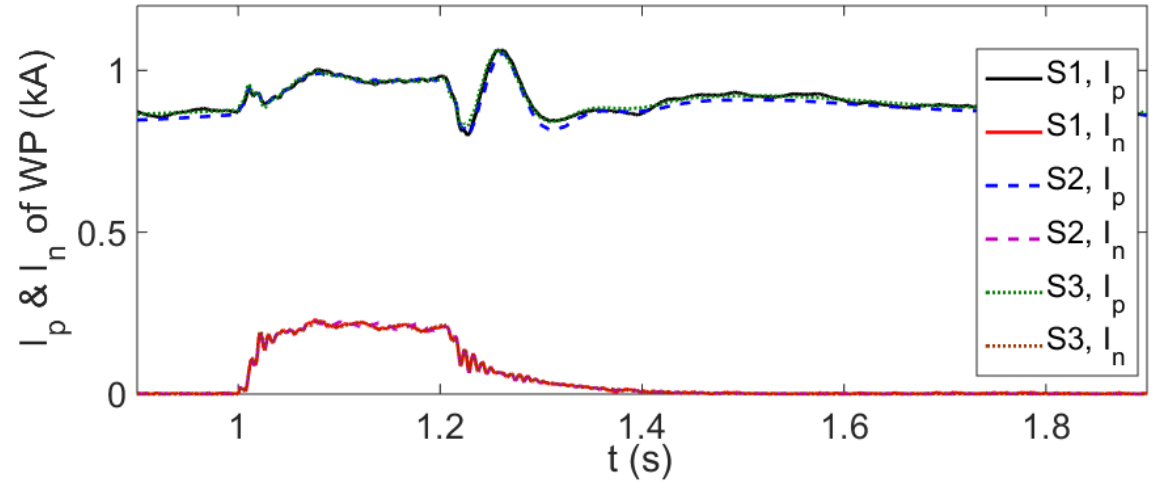

Figure 72 I_n and I_p of FSC WT based WP in IEEE 39 bus system simulation

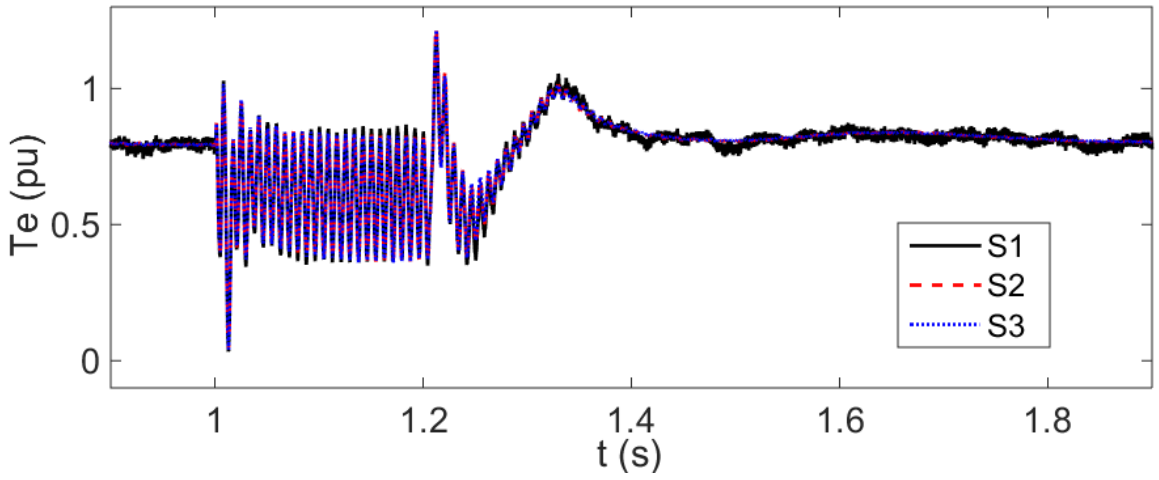

Figure 73 IG electromagnetic torque in IEEE 39 bus system simulation

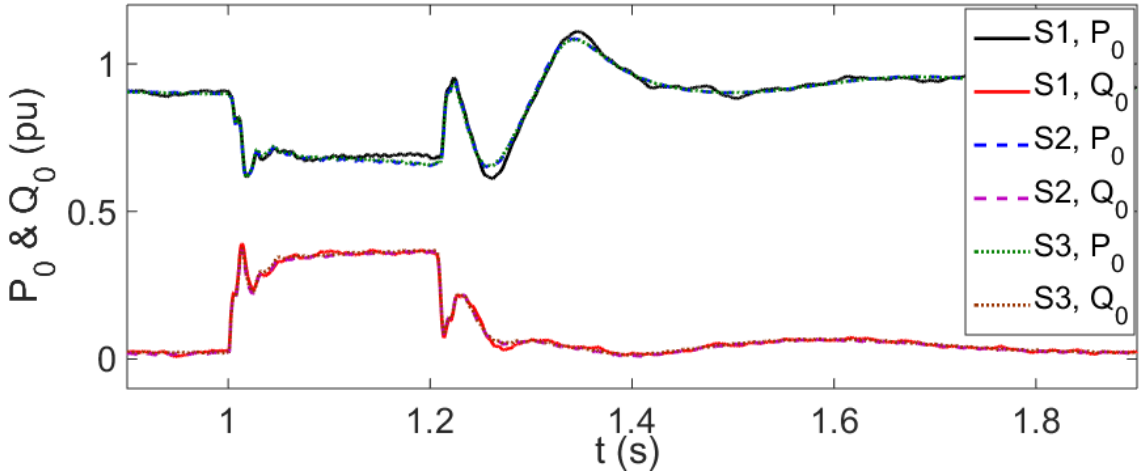

Figure 74 P_0 and Q_0 of aggregated DFIG WT in IEEE 39 bus system simulation

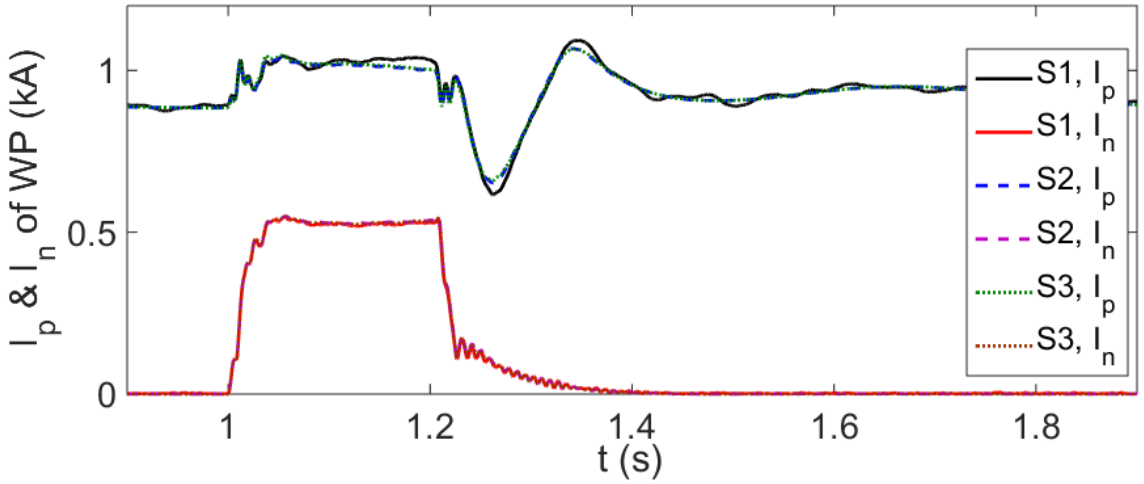

Figure 75 I_n and I_p of DFIG WT based WP in IEEE 39 bus system simulation

6 DETAILED WIND PARK MODELS AND AGGREGATED MODEL PRECISION

Certain grid integration studies, such as analysing collector grid faults and collector grid overcurrent protection system performance, LVRT and HVRT capability studies [1], ferroresonance study [29], require EMT type simulations with detailed wind park model. These studies do not only require detailed MW collector grid model, but also detailed model of HV/MV wind park substation including overvoltage protection, overcurrent and differential current protections, measuring current and voltage transformers as shown in Figure 76 - Figure 78.

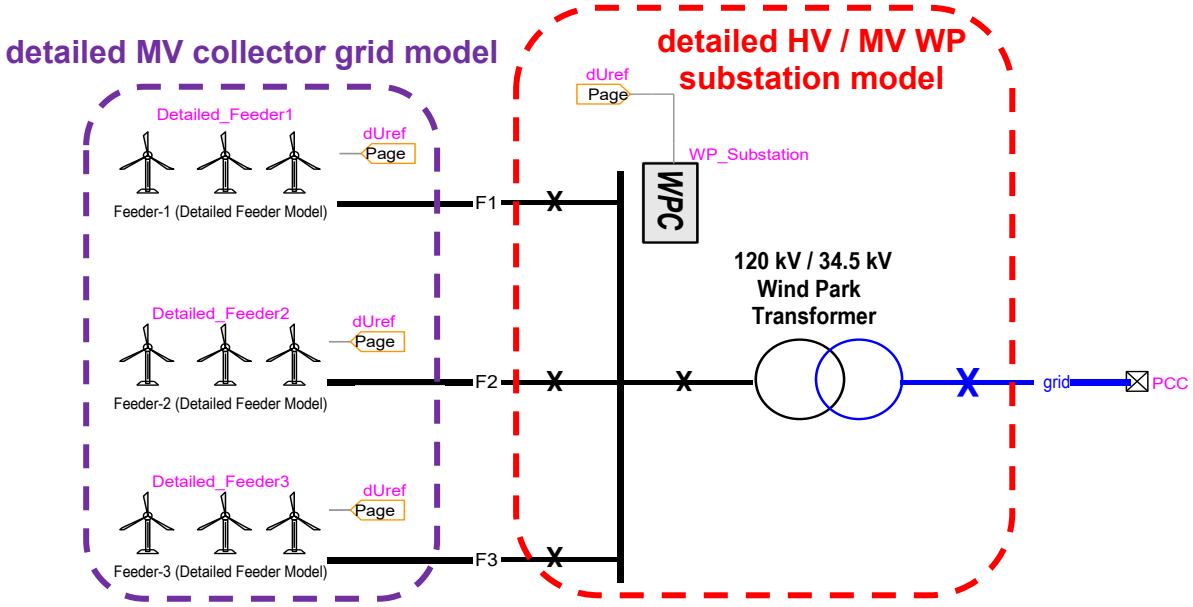

Figure 76 EMTP diagram of the 45 x 1.5 MW wind park detailed model given in Figure 46.

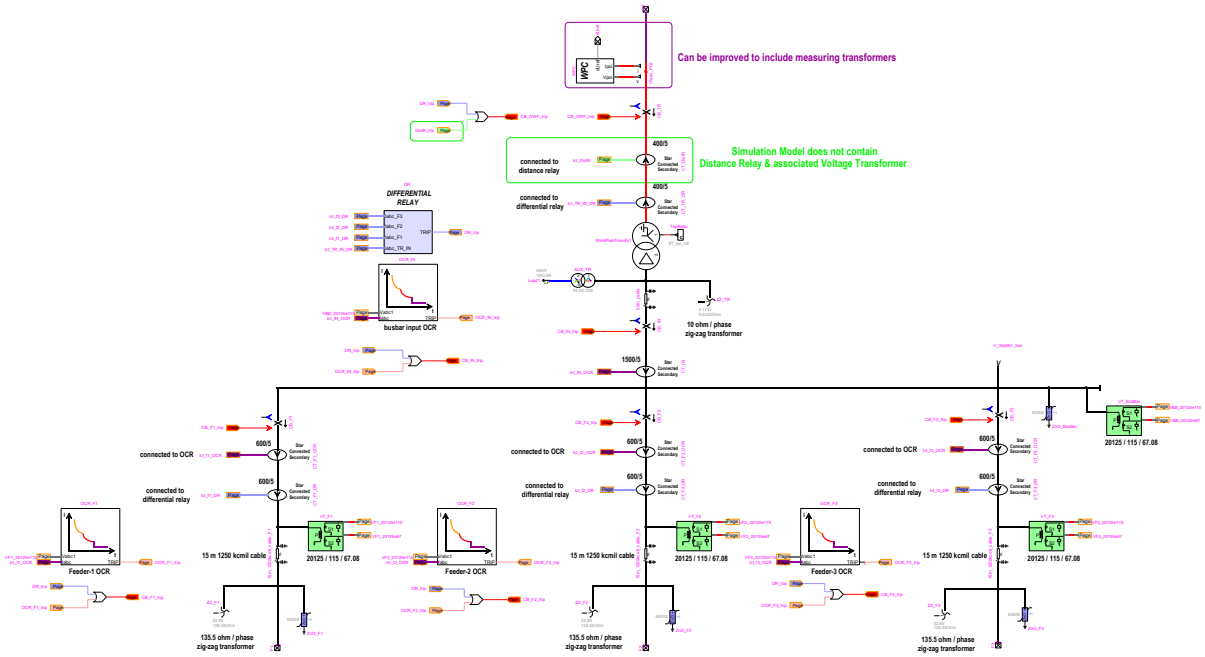

Figure 77 EMTP diagram of the HV/MV Wind Park Substation

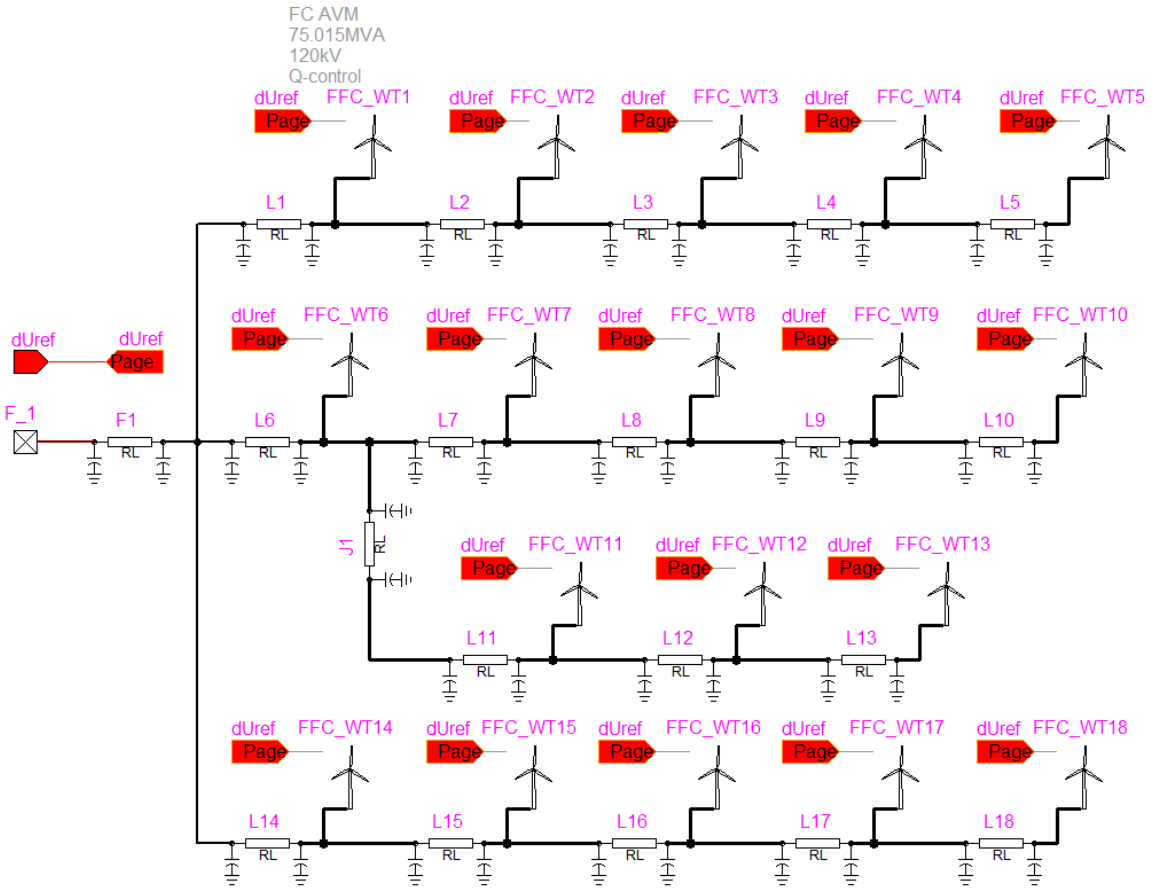

Figure 78 EMTP diagram of MV Feeder-1

The WT model in Figure 78 is obtained from the WP model presented in Chapter 3 by excluding the WPC, WP transformer and collector grid equivalent. The associated device mask is shown in Figure 79. It does not include the tabs used for MV/HV WP transformer and WPC parameters. On the other hand, the first tab of the aggregated wind turbine mask includes certain wind park parameters (total number of WTs in the WP, POI and collector grid voltage levels, collector grid equivalent and the MV/HV WP transformer impedances) in addition to the general wind turbine parameters (WT rated power, voltage and frequency) and wind speed. It should be noted that, the MV/HV WP transformer and the collector grid equivalent impedances are used GSC parameter calculation (see section 3.2.3.2).

Scenario M2 in Table I (DLG fault at BUS4 for GSC decoupled sequence control scheme) is simulated using the detailed wind park model to conclude on accuracy of the aggregated model. As shown in Figure 80 - Figure 83, the aggregated models of wind parks provide accurate results.

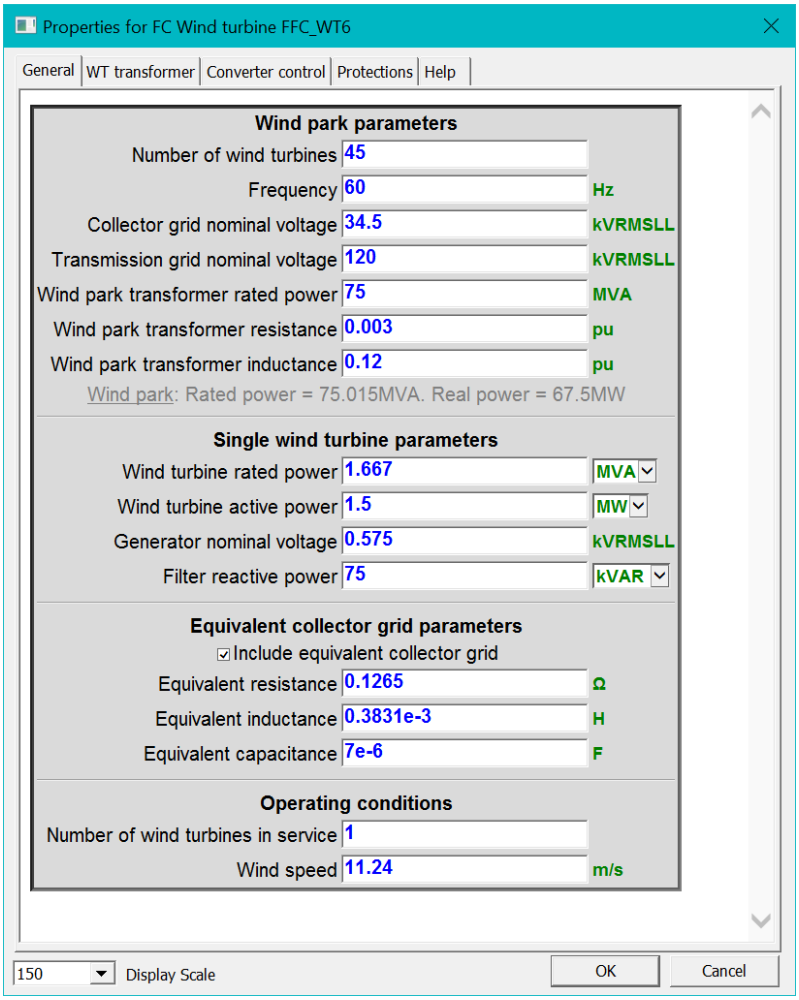

Figure 79 Aggregated FSC based wind turbine device mask

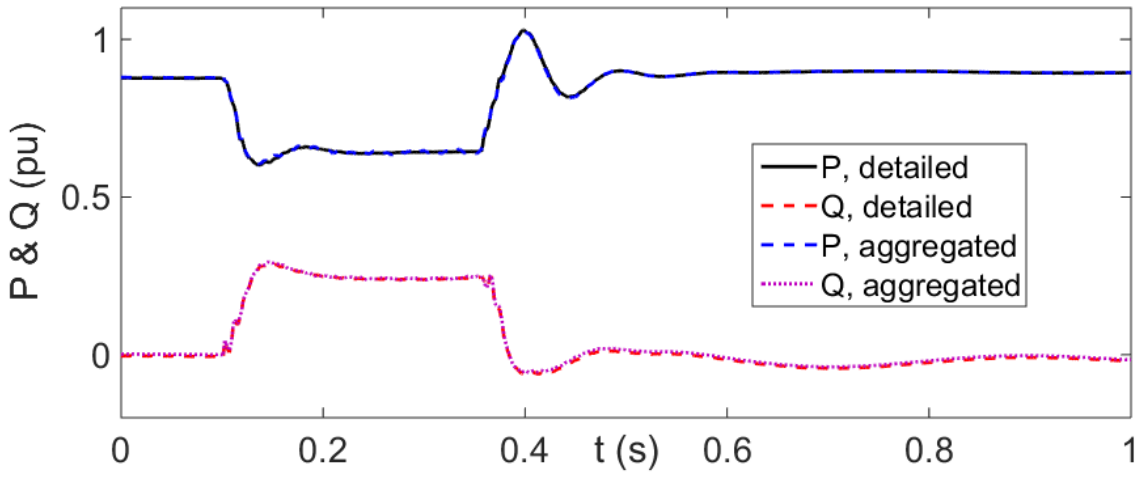

Figure 80 Active and reactive power at POI, Wind Park with FSC WTs

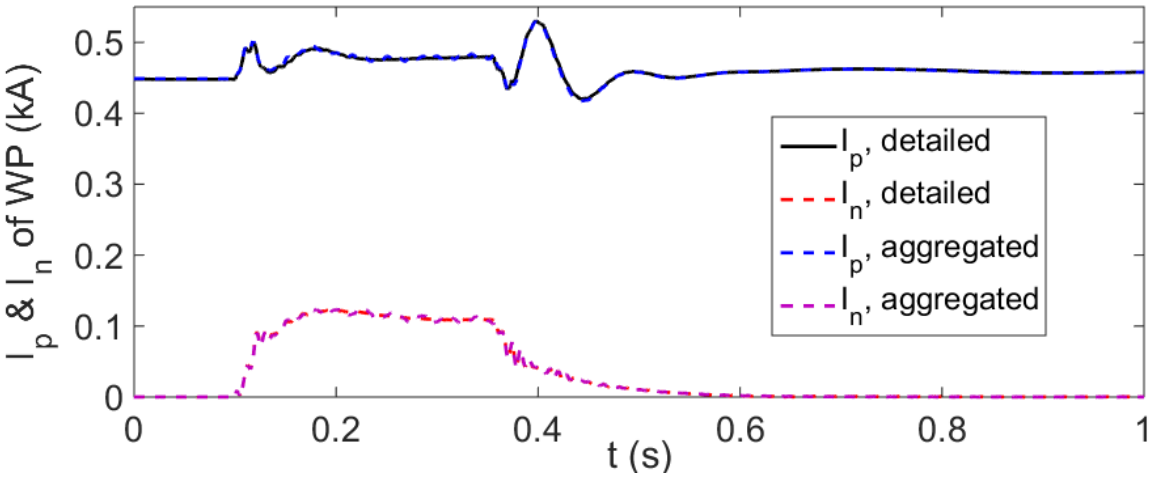

Figure 81 Positive and negative sequence currents at POI, Wind Park with FSC WTs

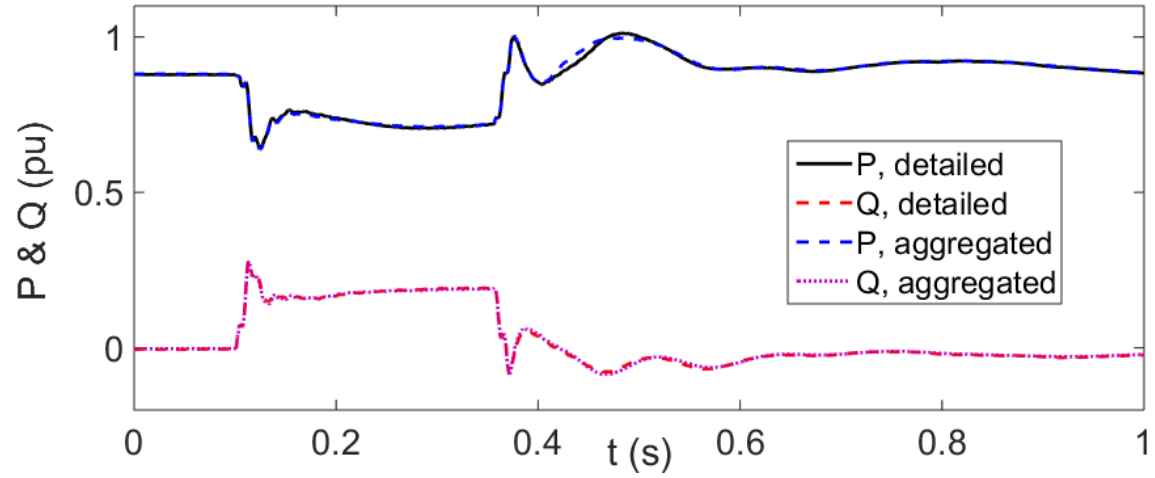

Figure 82 Active and reactive power at POI, Wind Park with DFIG WTs

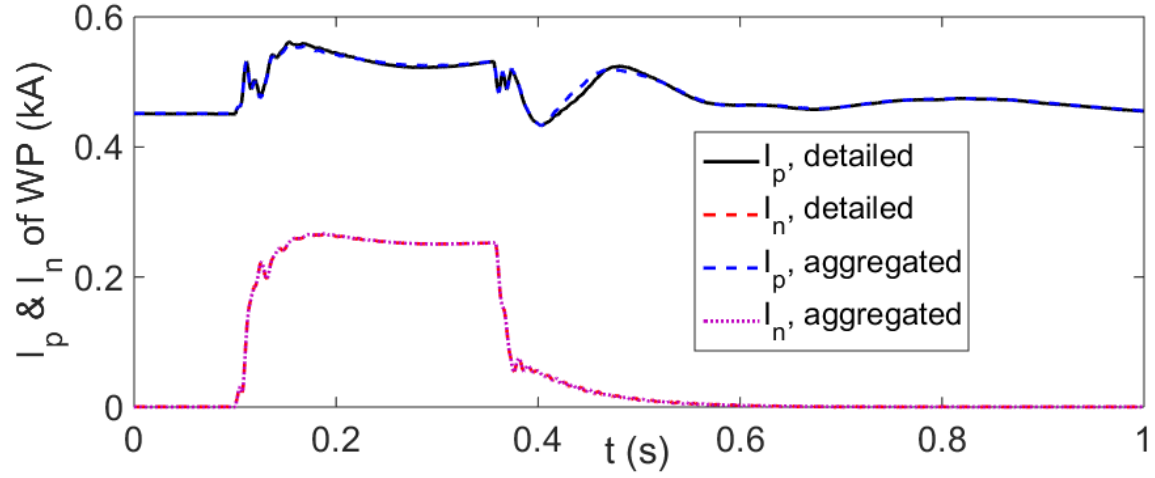

Figure 83 Positive and negative sequence currents at POI, Wind Park with DFIG WTs

7 REFERENCES

[1] U. Karaagac, J. Mahseredjian and L. Cai, “High Voltage Ride-Through Capability of DFIG-based Wind Parks with FACTS,” Proc. of 13th International Workshop on Large-Scale Integration of Wind Power into Power Systems, Berlin, Germany, Nov. 2014.

[2] O. Anaya-Lara, N. Jenkins, J. Ekanayake, P. Cartwright, and M. Hughes, Wind Energy Generation: Modelling and control, Wiley, 2009, John Wiley & Sons, Ltd.

[3] N. W. Miller, W. W. Price, and J. J. Sanchez-Gasca, “Dynamic modeling of GE 1.5 and 3.6 wind turbine-generators,” GE-Power System Energy Consulting, General Electric International, Inc., Schenectady, NY, USA, Oct. 2003.

[4] G. Abad, J. Lopez, M. A. Rodriguez, L. Marroyo, G. Iwanski, Doubly Fed Induction Machine: Modeling and Control for Wind Energy Generation, 2011, Wiley.

[5] M. Singh, S. Santoso, Dynamic Models for Wind Turbines and Wind Power Plants, 2011.

[6] J. M. Garcia, “Voltage control in wind power plants with doubly fed generators,” Ph.D. thesis, Alaborg Univ., Denmark, Sep. 2010.

[7] V. Akhmatov, A. H. Nielsen, J. K. Pedersen, O. Nymann, "Variable-speed wind turbines with multi-pole synchronous permanent magnet generators. Part I: Modelling in dynamic simualtion tools", Wind Eng., vol. 27, no. 6, pp. 531-548, Dec. 2003.

[8] S. R. Sanders, J. M. Noworolski, X. Z. Liu, and G. C. Verghese, “Generalized averaging method for power conversion circuits,” IEEE Trans. on Power Electron, vol. 6, no. 2, pp. 251–259, Apr. 1991.

[9] J. Morren, S. W. H. de Haan, P. Bauer, J. Pierik, and J. Bozelie, “Comparison of complete and reduced models of a wind turbine with Doubly-fed Induction Generator,” in Proc. 10th Eur. Conf. Power Electron. Appl., Toulouse, France, Sep. 2003.

[10] J. G. Slootweg, H. Polinder, and W. L. Kling, “Representing wind turbine electrical generating systems in fundamental frequency simulations,” IEEE Trans. on Energy Conv., vol. 18, no. 4, pp. 516-524, Dec. 2003.

[11] P. Rodriguez , J. Pou , J. Bergas , I. Candela , R. Burgos and D. Boroyevich, "Double synchronous reference frame PLL for power converters", Proc. IEEE PESC, pp. 1415-1421, 2005

[12] L. Harnefors and H. Nee, "Model-based current control of ac machines using the internal model control", IEEE Trans on Ind. Appl., pp. 133-141, Jan/Feb. 1998.

[13] “Grid code - high and extra high voltage,” E.ON Netz GmbH, Bayreuth, Germany, April 2006.

[14] R. Teodorescu, M. Liserre, P. Rodriguez, Grid Converters for Photovoltaic and Wind Power Systems, 2011, IEEE/Wiley.

[15] Rodriguez, P., Pou, J.,Bergas, J.,Candela, J. I.,Burgos,R.P. and Boroyevich, D., “Decoupled Double Synchronous Reference Frame PLL for Power Converters Control”, IEEE Transactions on Power Electronics, 22,March 2007, 584–592.

[16] Transmission Provider Technical Requirements for the Connection of Power Plants to the Hydro-Quebec Transmission System, Hydro Quebec Transenergie, 2009.

[17] G. R. Slemon, “Modelling of induction machines for electric drives,” IEEE Transactions on Industry Applications, 25(6):1126-31, 1989.

[18] R. Pena, J. C. Clare, G.M. Asher, “Doubly fed induction generator using back to back PWM converters and its application to variable-speed wind-energy generation”, IEE Proc. Electr. Power Appl., No.3. pp.231-240, 1996.

[19] Muljadi, T. Batan, D. Yildirim, C. Butterfield, “Understanding the unbalanced voltage problem in wind turbine generation Proc. Ind. Appl. Conf., pp. 1359–1365.

[20] T.K.A. Brekken, N. Mohan, “Control of a doubly fed induction wind generator under unbalanced grid voltage conditions,” IEEE Trans. Energy Convers., Vol: 22, No: 1, pp. 129-135, March 2007.

[21] L. Xu, Y. Wang, “Dynamic modeling and control of DFIG-based wind turbines under unbalanced network conditions,” IEEE Trans. Power Syst., Vol: 22, No: 1, pp. 314-323, Feb. 2007.

[22] R. Pena, R. Cardenas, E. Escobar, “Control system for unbalanced operation of stand-alone doubly fed induction generators,” IEEE Trans. Energy Convers., Vol: 22, No: 2, pp. 544–545, June 2007.

[23] H. Yin, L. Fan, R. Kavasseri, “Negative sequence compensation techniques of dfig-based wind energy systems under unbalanced grid conditions,” Proc. IEEE Power Electronics and Machines in Wind Applications (PEMWA), Lincoln, NE, 2009.

[24] L. Fan, H. Yin, Z. Miao, “A novel control scheme for DFIG-based wind energy systems under unbalanced grid conditions,” Electric Power Systems Research, Vol: 81, No:2, pp. 254–262, Feb. 2011.

[25] T. Kauffmann, U. Karaagac, I. Kocar, H. Gras, J. Mahseredjian, B. Cetindag and E. Farantatos, “Phasor Domain Modeling of Type III Wind Turbine Generator for Protection Studies,” Proc. of IEEE PES General Meeting, Denver, CO, USA, July 2015

[26] U. Karaagac, T. Kauffmann, I. Kocar, H. Gras, J. Mahseredjian, B. Cetindag and E. Farantatos, “Phasor Domain Modeling of Type-IV Wind Turbine Generator for Protection Studies,” Proc. of IEEE PES General Meeting, Denver, CO, USA, July 2015.

[27] T. Kauffmann; U. Karaagac; I. Kocar; S. Jensen; J. Mahseredjian; E. Farantatos, "An Accurate Type III Wind Turbine Generator Short Circuit Model for Protection Applications," in IEEE Trans. on Power Delivery, doi: 10.1109/TPWRD.2016.2614620.

[28] E. Muljadi, C.P. Butterfield, a Ellis, J. Mechenbier, J. Hochheimer, R. Young, N. Miller, R. Delmerico, R. Zavadil and J.C. Smith, "Equivalencing the collector system of a large wind power plant", 2006 IEEE PES General Meeting.

[29] U. Karaagac, J. Mahseredjian, L. Cai, “Ferroresonance conditions in wind parks”, Electric Power Systems Research, Vo: 138, pp 41-49, Sep. 2016.